Theses and Dissertations

2016

Utilization Of Satellite-Derived Salinity For ENSO Studies And Climate Indices

Caroline Mary Corbett
University of South Carolina

UTILIZATION OF SATELLITE-DERIVED SALINITY FOR ENSO STUDIES AND CLIMATE INDICES

by

Caroline Mary Corbett

Bachelor of Science
Saint Louis University, 2015

_____

Submitted in Partial Fulfillment of the Requirements

For the Degree of Master of Science in

Geological Sciences

College of Arts and Sciences

University of South Carolina

2016

Accepted by:

Subrahmanyam Bulusu, Director of Thesis

Venkat Lakshmi, Reader

Alexander Yankovsky, Reader

Camelia Knapp, Reader

Cheryl L. Addy, Vice Provost and Dean of the Graduate School

ii

ACKNOWLEGEMENTS

ABSTRACT

Conventionally, El Niño-Southern Oscillation (ENSO) is studied using sea surface temperature (SST) observations in the central and eastern equatorial Pacific Ocean. Recently, sea surface salinity (SSS) in the equatorial Pacific has been studied in relation to the phases of ENSO. Previously, SSS was observed in the equatorial Pacific using the Tropical Ocean Global Atmosphere (TOGA) / Tropical Atmosphere Ocean (TOA), the Argo float network, and Oceanic General Circulation Models (OGCM). The launch of NASA's Aquarius Salinity Mission and ESA's Soil Moisture Ocean Salinity (SMOS) opened a new era in which high resolution global near real-time SSS observations are readily available. These satellites have made the collection and analysis of SSS data easier and have improved our understanding of salinity variability during ENSO.

This study examines the accuracy and validity of the Aquarius and SMOS SSS datasets and compares them to the Argo float observations. This comparison shows that the three datasets are comparable, although there are some discrepancies. These differences are mainly focused in the regions of upwelling and high precipitation. The performance of these datasets is analyzed specifically during the 2014-15 ENSO event. Their observations are comparable during this event, but there are notable differences. These salinity discrepancies cannot be explained with evaporation and precipitation patterns (E-P).

Further examination of the 2014-15 ENSO event is conducted, and it is compared to the strong 1997-98 El Niño event and the similarly failed 2012-13 ENSO event. This study demonstrates that both E-P variability and anomalously eastward surface currents are required for the full development of El Niño conditions. It is also essential that anomalous fresh SSS migrate eastward of the International Date Line in order for a successful El Niño to occur. Observed SSS variability in the equatorial Pacific is clearly linked to the onset and death of El Niño conditions.

Finally, a new index called the Western Pacific Salinity Index (WPSI) is developed based on the SSS variability observed in the region defined from 5°N to 5°S and 160°E to 170°W. When calculated using Argo and SMOS SSS data, this index is capable of identifying warm, cool, and neutral phases of ENSO. However, the Aquarius dataset is less capable of observing the phases of ENSO. WPSI is highly correlated to other ENSO indices that are commonly used for monitoring and forecasting.

TABLE OF CONTENTS

LIST OF TABLES

LIST OF FIGURES

CHAPTER 1

INTRODUCTION

1.1 STUDY AREA

The equatorial Pacific Ocean is the focus study area for this research. This region is generally defined from 5°N to 5°S, 120°E to 70°W, a region which is diverse in sea surface temperature (SST) and sea surface salinity (SSS). The western Pacific warm pool dominates the western equatorial Pacific. Convection over the warm SSTs of the western Pacific warm pool causes large amounts of precipitation over the region (Delcroix et al., 1996; Chen et al., 2004; Cravatte et al., 2009); therefore, this region is also characterized by fresh SSS (Cravatte et al., 2009; Qu et al., 2014).

The eastern equatorial Pacific is dominated by cool SSTs, higher saline, and nutrient rich waters; this is due to upwelling off the coast of South America (Chavez et al., 1999). Although these are the mean conditions in the equatorial Pacific Ocean, they are altered significantly during El Niño-Southern Oscillation.

1.2 EL NIÑO-SOUTHERN OSCILLATION

El Niño-Southern Oscillation (ENSO) is a climate scale phenomena that occurs in the equatorial Pacific Ocean and has global oceanic and atmospheric impacts (Singh et al., 2011; Menkes et al., 2014; Capotondi et al., 2015; McPhaden, 2015). ENSO has three phases: the warm phase, called El Niño, the cool phase, called La Niña, and the neutral phase.

1

During El Niño, warm SSTs from the western Pacific warm pool are zonally displaced eastward (Trenberth, 1997; Singh et al., 2011; Qu and Yu, 2014). Anomalously warm SSTs migrate to the coast of South America, cutting off the equatorial upwelling that occurs in the region (Trenberth, 1997). This affects the nutrient supply and severely impacts biological processes and diversity (Trenberth, 1997; Chavez et al., 1999). In the atmosphere during El Niño, the Hadley and Walker cells are altered. This causes anomalously high precipitation over the western and central Pacific. Additional atmospheric changes occur globally and the effects are observed in regions such as North America and Africa. Furthermore, El Niño conditions are linked to high sea surface height (SSH) observations in the eastern equatorial Pacific and linked to equatorial Kelvin Wave patterns (Picaut and Delcroix, 1995; Picaut et al., 2002).

Oppositely, during La Niña, anomalously warm SSTs migrate westward and the eastern equatorial Pacific is dominated by an anomalously large equatorial Pacific "cold tongue" (Hasson et al., 2014). This region is nutrient rich, fueled by increased upwelling off the coast of South America (Chavez, 1999; Hasson et al., 2014). The Walker Circulation is altered during La Niña conditions, which affects the precipitation patterns in the western Pacific (Hasson et al., 2014). Additionally, La Niña conditions are linked to Rossby Wave patterns (Picaut and Delcroix, 1995; Picaut et al., 2002).

1.3 SEA SURFACE SALINITY

ENSO is usually observed using SSH and SST anomalies throughout the equatorial Pacific. Recently it has been discovered that SSS also varies during the warm

2

and cool phases of ENSO. A number of new mechanisms for SSS measurement allow for easier, more extensive, and long-term analysis of the SSS variability.

SSS is an important variable to study generally and in connection to El Niño. SSS can be used as a proxy for evaporation minus precipitation (E-P), because SSS increases when evaporation dominates and SSS decreases when precipitation dominates (Yu, 2011). Unlike SST, SSS is unaffected by the diurnal cycle and varies at a slower timescale (Spall, 1992; Yu, 2011; Qu and Yu, 2014).

SSS during ENSO is not well understood but has been studied more with increasing access to global and high-resolution measurements. The launch of NASA's Aquarius Salinity Mission and ESA's Soil Moisture Ocean Salinity (SMOS) have provided global satellite derived SSS data since 2010. In association with the expansive Argo float network and oceanic models, these satellite observations can be used to expand our understanding of SSS variability.

Chapter 2 validates the use of Aquarius and SMOS SSS data as compared to Argo near-surface salinity data in the equatorial Pacific generally and during the 2014-15 ENSO event. This study reveals the biases of both satellites as compared to Argo and shows that the satellites are comparable in this region. However, the Aquarius Mission ended in June 2015, leaving SMOS as the most useful satellite tool still in operation for the study of SSS in the equatorial Pacific during ENSO.

Chapter 3 is a comparison study of the strong 1997-98 El Niño, and the failed 2012-13 and 2014-15 ENSO events. This study identifies the importance of and need for both anomalous E-P and anomalous surface currents in the SSS variability to initiate a successful El Niño event. The lack of one of these variables is recognized as an important

3

factor in the failure of the 2012-13 and 2014-15 ENSO events. Additionally, the International Date Line is identified as an important marker, as anomalously fresh SSS must migrate east of it during a fully formed and long lasting El Niño event.

Lastly, Chapter 4 summarizes the major findings of this work. The use of these findings for future research into and development of SSS ENSO indices is presented and discussed. The findings from Chapters 2 and 3 can be implemented into SSS indices for ENSO forecasts. A new SSS ENSO index called the Western Pacific Salinity Index (WPSI) is introduced. The calculation of the index is conducted using the Argo, Aquarius, and SMOS datasets. WPSI is shown to be capable of identifying the three phases of ENSO when calculated using Argo and SMOS.

4

CHAPTER 2

VALIDATION OF SATELLITE-DERIVED SALINITY IN THE EQUATORIAL

PACIFIC WITH SPECIFIC EMPHASIS ON THE 2014-15 ENSO EVENT[1]

---

[1]Corbett, C.M. and B. Subrahmanyam. 2016. *IEEE Geosci. Remote Sens Lett.*
 doi:10.1109/LGRS.2016.2619980.

ABSTRACT

This letter compares satellite and *in situ* sea surface salinity (SSS) measurements in the tropical Pacific Ocean and validates the performance of satellite products during the 2014–15 El Niño-Southern Oscillation (ENSO) event. SSS measurements from NASA's Aquarius Salinity Mission and the European Space Agency's Soil Moisture and Ocean Salinity (SMOS) are compared with Argo float data. This comparison shows that the Aquarius and SMOS satellites are generally able to resolve the SSS in the tropical Pacific, despite some discrepancies in regions of upwelling and high precipitation. The two satellites perform better with respect to Argo in Niño 4 than in Niño 3 and Niño 1 + 2. However, in each region, Aquarius and SMOS are highly correlated with each other. During the 2014–15 ENSO event, each dataset observes similar SSS, although some discrepancies exist. Analysis of anomalous evaporation minus precipitation during this event demonstrates that the differences between each dataset are not fully explained by precipitation patterns.

2.1 INTRODUCTION

Salinity variability is known to play an important role in ocean dynamics (Rao and Sivakumar, 2003; Foltz and McPhaden, 2008; Yu, 2011; Bingham et al., 2012). Sea surface and near surface salinity variability is closely related to evaporation minus precipitation (E-P) and can be used as a proxy for the global water cycle (Delcroix et al., 1996; Yu, 2011; Nyadjro and Subrahmanyam, 2014). In the tropical Pacific, precipitation

6

dominates the intertropical convergence zone (ITCZ) and the South Pacific convergence zone (SPCZ). These two regions meet in the western equatorial Pacific, at the western Pacific warm pool. Low sea surface salinity (SSS) is found along the ITCZ, SPCZ, and in the western Pacific warm pool due to the rainfall in these regions (Delcroix et al., 1996; Vialard et al., 2002; Yu, 2011; Qu et al., 2014).

SSS and E-P in the tropical Pacific are altered during the phases of El Niño-Southern Oscillation (ENSO). The western Pacific warm pool and the associated fresh pool are zonally displaced eastward during El Niño (Trenberth, 1997; Singh et al., 2011). Changes in the Walker and Hadley cells during ENSO cause anomalously high precipitation over the western and central Pacific (Lau and Chan, 1983; Delcroix et al., 1996). Understanding SSS variability during El Niño is important for the ocean-atmosphere coupling during events. SSS and thus salinity stratification are partially affected by anomalous E-P patterns in the tropical Pacific. Salinity stratification and barrier layer formation are understood to greatly influence El Niño formation (Maes et al., 2002; Maes et al., 2004; Qu et al., 2014).

Until recently, global SSS measurements have been sparse. The Argo float network provides global near surface salinity measurements throughout the oceans. However, float population is scarce in many areas around the world. With the launch of NASA's Aquarius Salinity Mission, which ended June 7, 2015, and the European Space Agency's Soil Moisture Ocean Salinity (SMOS), which is still operational, global high-resolution SSS data is now more readily available. Argo, Aquarius, and SMOS salinity products are frequently used to study the tropical Pacific and the phases of ENSO.

7

In this letter, we compare the Argo, Aquarius and SMOS SSS data sets and their performance in the tropical Pacific. Specifically, the performance of the two satellites is assessed in comparison to Argo during the 2014–15 El Niño. The unusual progression of this event makes it an interesting case study for satellite validation. The results of this letter aim to assess the validity of the Aquarius and SMOS data sets in the tropical Pacific generally and during El Niño events. We also aim to advance our understanding of the SSS variability during the irregular 2014–15 El Niño event.

2.2 DATA AND METHODS

In this letter, we use International Pacific Research Center processed monthly Argo SSS data obtained from the Asia-Pacific Data-Research Center (http://apdrc.soest.hawaii.edu/projects/argo/). These data are produced by optimal interpolation with a spatial resolution of 1° × 1° and are available from January 2005 to June 2016. We use monthly Aquarius version 4.0 Level 3 SSS data at a 1° × 1° spatial resolution obtained from NASA Jet Propulsion Laboratory (JPL) Physical Oceanography Distributed Active Archive Center (PO.DAAC) (http://podaac.jpl.nasa.gov/aquarius). The Aquarius mission ended in June 2015 and the monthly data set is available from August 2011 to May 2015. SMOS version 2.0 Level 3 monthly SSS data at a 0.25° × 0.25° spatial resolution is used and obtained from Barcelona Expert Centre (http:// cp34-bec.cmima.csic.es/). These data are available from January 2010 to June 2016, although the mission is still in operation. Olmedo et al., (2016) provide detailed information about methods by which this product was processed. For comparisons with Argo and Aquarius, the horizontal resolution of SMOS is reduced to 1° × 1°.

8

We use evaporation and precipitation data from the European Centre for Medium-Range Weather Forecasts (ECMWF) ERA-Interim global atmospheric reanalysis (http://apps.ecmwf.int/datasets/data/interim-fullmnth/levtype=sfc/). These data are synoptic monthly means at a 1° × 1° spatial resolution and are available from January 1979 to April 2016. For surface currents, we use the Ocean Surface Current Analyses Real-time (OSCAR) at a 0.33° × 0.33° spatial resolution, which is available through NASA JPL PO.DAAC. These data are available from October 1992 to December 2015 in a 5-day cycle format. For this letter, we converted to a monthly format and reduced the spatial resolution to 1° × 1° to match the salinity data sets.

From August 2011 to May 2015, Argo, Aquarius, and SMOS were all operational. This time period is used for comparison and statistical analysis of the three data sets. For each data set, anomalies are calculated by removing the monthly means. Monthly means are calculated by averaging monthly data over the entire span on the data set.

It is important to discuss the differences between Argo in situ measurements and satellite products before conducting the validation. Argo floats measure salinity from 5 to 2000 m depth and measurements are not taken above 5 m (Moon et al., 2014; Qu et al., 2014; Song et al., 2015). Therefore, Argo SSS is more accurately described as near-surface salinity measurements (Lagerloef et al., 2008; Riser et al., 2008; Henocq et al., 2010; Boutin et al., 2013; Qu et al., 2014). On the other hand, satellites observe skin measurements of salinity, which is approximately equal to the top 5 cm of the ocean (Moon et al., 2014; Song et al., 2015). Surface and near-surface salinity can vary significantly. This is most notably due to rainfall-induced surface freshwater pooling (Lagerloef et al., 2008; Riser et al., 2008; Henocq et al., 2010; Boutin et al., 2013; Moon

et al., 2014; Song et al., 2015). Therefore, discrepancies in the data sets can arise from the differences in measurement depth. Additional causes for error are discussed later.

2.3 RESULTS

2.3.1 ASSESSMENT OF AQUARIUS AND SMOS

To assess the validity of Aquarius and SMOS SSS in the tropical Pacific, we compare them to Argo. Generally, the three data sets observe the same mean SSS (Figure 2.1). Subtle differences between the data sets are realized when the satellite data sets are subtracted from Argo and when SMOS is subtracted from Aquarius.

Argo has a salty bias, greater than 0.45 psu, along the ITCZ over the region. As discussed, satellites are affected by precipitation induced surface freshwater pooling because they measure the top 5 cm of the ocean surface. Alternatively, Argo profilers measure at 5 m depth and SSS is extrapolated to the surface (Lagerloef et al., 2008; Riser et al., 2008; Henocq et al., 2010; Boutin et al., 2013; Qu et al., 2014). Compared to Aquarius, Argo has a salty bias off the coast of Panama (Figure 2.1D). Argo has a salty bias over SMOS off the coast of Panama and much of South America (Figure 2.1E). Argo has a fresh bias of the order of −0.55 psu along the rest of the Central American coastline (Figure 2.1D, E). Land contamination and the scarcity of Argo floats in this region could be contributing to this.

Aquarius has a small salt bias off Peru (Figure 2.1D). SMOS has a larger salt bias, of the order of 0.35 psu, along the equator from 140° W to the coast of South America (Figure 2.1E). Compared to Aquarius, SMOS has a fresh bias along the coast of Central and South America and throughout Oceania, which is likely a result of land

10

contamination (Figure 2.1F). SMOS also has a fresh bias along portions of the ITCZ and SPCZ. SMOS has a salt bias along the equator, which is likely due to upwelling (Qu et al., 2014). This SMOS salt bias is also documented by (Maes et al., 2014).

Evaporation and precipitation patterns in Figure 2.2 match results found in Delcroix et al., (1996), Vialard et al., (2002), Yu, (2011), and Qu et al., (2014). Negative E-P, resulting from more precipitation than evaporation, occurs along the ITCZ and SPCZ and over the western Pacific warm pool. Significant E-P anomalies occur along the coast of Panama, Columbia, and Ecuador. This is the region where Argo observes saltier salinities than the satellites. Near zero and weakly positive E-P occurs along the equator, where SMOS observes saltier salinities than Argo and Aquarius.

Argo and Aquarius appear to measure similar SSS in the equatorial Pacific, Niño 4 and Niño 3 (Figure 2.3A, B, C). SMOS observes fresher SSS in the equatorial Pacific and Niño 4, but is similar to Argo and Aquarius in Niño 3. However, all three data sets agree on the general trends of SSS in these regions. In Niño 4, all data sets agree on the steepness and timing of the decrease in SSS in early 2014. Less agreement occurs in Niño 1 + 2, where SMOS again observes fresher SSS (Figure 2.3D). SSS anomalies appear to correlate well in each of the regions (Figure 2.3E-H). Discrepancies that exist are on the order of 0.2 psu or less. The largest differences between anomalies are seen in Niño 1 + 2.

Statistical analysis of Argo, Aquarius and SMOS anomalies was performed (Table 2.1, Figure 2.4). Aquarius consistently performs better than SMOS when compared to Argo. The lowest standard deviations and root-mean-square deviations (RMSDs) and the highest correlations between all data sets are found in the equatorial

Pacific and Niño 4. Compared to the other regions, the satellites perform poorly with respect to Argo in Niño 3 and Niño 1 + 2. For each comparison, the largest standard deviations and RMSDs are in Niño 1 + 2. These results indicate that Aquarius and Argo are most similar across the Pacific, but SMOS is still comparable.

2.3.2 SEA SURFACE SALINITY DURING THE 2014-15 ENSO EVENT

The 2014–15 El Niño is rather distinctive. In early 2014, a strong El Niño was forecasted but failed to fully form. In 2015, the El Niño unexpectedly regenerated and became one of the strongest El Niño events on record (McPhaden, 2015). The stalling in 2014 and the regeneration of the El Niño in 2015 make the progression of this event unique.

During this event, Argo, Aquarius, and SMOS appear to observe similar SSS (Figure 2.5). All three data sets tend to agree on the location of negative and positive anomalies. Argo tends to see larger regions of negative and positive anomalies than Aquarius. SMOS tends to show more detail and observes fresher anomalies in the regions of negative anomalies. The largest discrepancies between the data sets are found in the ITCZ, SPCZ, and off the coast of Central and South America. This coincides with discrepancies between datasets in Figure 2.1.

Correlations between Argo, Aquarius, and SMOS during each month in the tropical Pacific are calculated but not shown. Statistically, Argo is minimally correlated with Aquarius and SMOS (less than 0.28 correlation coefficient) during each month. SMOS and Aquarius are highly correlated, with correlation coefficients greater than 0.56.

12

Errors during this event are calculated in the equatorial Pacific, Niño 4, Niño 3, and Niño 1 + 2 regions but also not shown. In each of the regions, the data sets are less correlated during this event than they are from August 2011 to May 2015 (Table 2.1, Figure 2.4). All data sets are strongly correlated in the equatorial Pacific, and Niño 4 and weakly correlated in Niño 3. In Niño 1 + 2, only Aquarius and SMOS are strongly correlated and the satellite data sets are not correlated to Argo.

Negative E-P anomalies over the ITCZ and SPCZ vary throughout the event but can generally explain the observed SSS differences (Figure 2.6). Positive E-P anomalies tend to dominate along the equator, where the three data sets are strongly correlated in Niño 4. This indicates that the three data sets perform well with respect to each other due to the lack of precipitation.

Negative E-P anomalies near Panama, Columbia, and Ecuador cannot explain the observed SSS discrepancies, as Argo tends to observe fresher anomalies. Near normal conditions and weakly positive E-P anomalies are seen in Niño 3 and Niño 1 + 2; SSS discrepancies and lack of correlation are likely explained by upwelling conditions in and around this region.

2.4 CONCLUSION

The modification and role of SSS in the tropical Pacific during El Niño is increasingly studied. Atmospheric and oceanic changes during El Niño alter SSS patterns and E-P throughout the tropical Pacific. Understanding this SSS variability is important for characterizing the dynamical changes that occur during these events. Satellite measured SSS data had greatly improved our ability to study SSS during ENSO. Here,

13

we have compared Aquarius and SMOS to Argo to validate the accuracy of the salinity data sets in the tropical Pacific. We then examined their performance specifically during the unique 2014–15 El Niño event. E-P variability was assessed as a possible cause for the disagreements between data sets.

Typically, satellites observe fresher anomalies than Argo in regions of significant precipitation. This was found to be true over much of the ITCZ and SPCZ, where Argo has a salty bias. Significant negative E-P along the coast of Panama, Columbia, and Ecuador explain the satellite fresh bias. The satellites have a salt bias over the region of upwelling off the Peruvian coast.

When using these data sets to study the 2014–15 El Niño, these biases are important to note. SSS discrepancies between Argo, Aquarius, and SMOS during this event most notably occur in the ITCZ, SPCZ, and off the coast of Central and South America. Anomalous E-P cannot always explain these salinity differences.

In the ITCZ and SPCZ, anomalously negative E-P can explain SSS discrepancies. However, anomalously negative E-P is seen off the coast of Panama, where Argo observes more negative SSS anomalies than the satellites. Near normal and slightly positive E-P anomalies are observed in the Niño 3 and Niño 1 + 2 regions, despite a lack of correlation between Argo and the satellites. Therefore, precipitation patterns cannot completely reconcile the disagreements between data sets. Consequently, differences between Argo and satellite observations must be discussed and taken into account.

There are numerous possible explanations for disagreements between Argo and satellite observations. The first is the depth sampling differences between Argo and satellites. The topmost salinity measurement with Argo floats occurs at 5 m depth, while

14

satellites observe salinity in the top 5 cm. Differences in surface and subsurface SSS variability caused by freshwater fluxes may be driving the discrepancies between Argo and satellite observations (Moon et al., 2014; Song et al., 2015). Second, the relatively coarse Argo observations, compared to satellites, and the differences in sampling times between the products may also factor into the differences (Boutin et al., 2016). Land contamination from satellite observations in the Niño 1 + 2 region may also factor into the observed discrepancies.

Overall, the comparisons between the three data sets are favorable. Argo, Aquarius, and SMOS generally agree on the large scale SSS patterns in the equatorial Pacific. However, the biases are important to take into account when analyzing smaller regions, specifically along the ITCZ, SPCZ, and the coast of Central and South America. During El Niño, the data sets are still strongly correlated, but disagreements become problematic when observing SSS in the eastern Niño regions.

As the SMOS mission continues its operation, additional studies of SSS variability in the equatorial Pacific can be conducted. Future El Niño events can be studied in detail using Argo, SMOS, and the new Soil Moisture Active Passive (SMAP) mission, which will also provide salinity data for the region.

Table 2.1. Comparison of the Argo, Aquarius, and SMOS anomalies with respect to the mean taken from August 2011 to May 2015 in the equatorial Pacific (5°N-5°S, 130°E-90°W), Niño 4 region (5°N-5°S, 160°E-150°W), Niño 3 region (5°N-5°S, 150°-90°W), and Niño 1 + 2 region (0°-10°S, 90°-80°W)

		Standard Deviation	RMSD	Correlation Coefficient
Eq Pacific	Argo vs. Aquarius	0.25	0.15	0.79
	Argo vs. SMOS	0.25	0.17	0.73
	Aquarius vs. SMOS	0.25	0.15	0.82
Niño 4	Argo vs. Aquarius	0.22	0.11	0.87
	Argo vs. SMOS	0.26	0.14	0.83
	Aquarius vs. SMOS	0.26	0.13	0.86
Niño 3	Argo vs. Aquarius	0.23	0.17	0.70
	Argo vs. SMOS	0.22	0.18	0.62
	Aquarius vs. SMOS	0.22	0.14	0.80
Niño 1+2	Argo vs. Aquarius	0.32	0.23	0.70
	Argo vs. SMOS	0.35	0.27	0.64
	Aquarius vs. SMOS	0.33	0.20	0.82
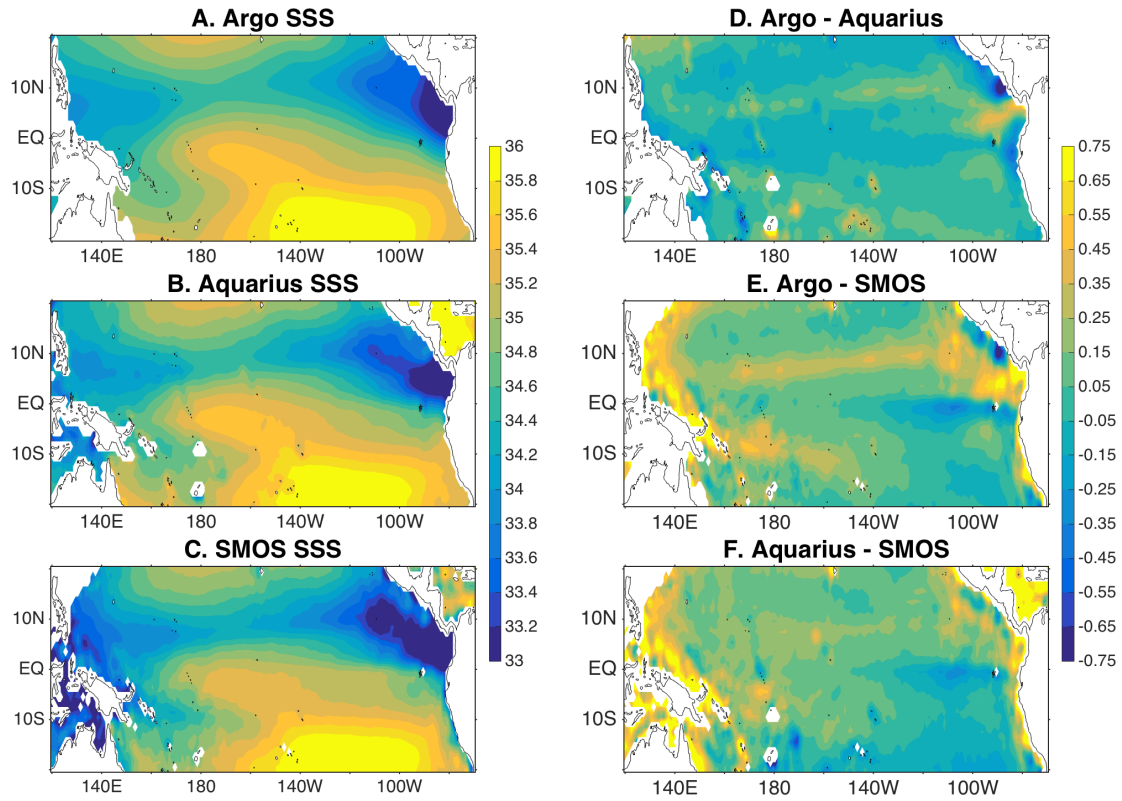
Figure 2.1. Mean SSS (psu) from August 2011 to May 2015 for (A) Argo and (B) Aquarius and (C) SMOS. Difference in mean SSS (psu) for (D) Argo and Aquarius, (E) Argo and SMOS, and (F) Aquarius and SMOS

17
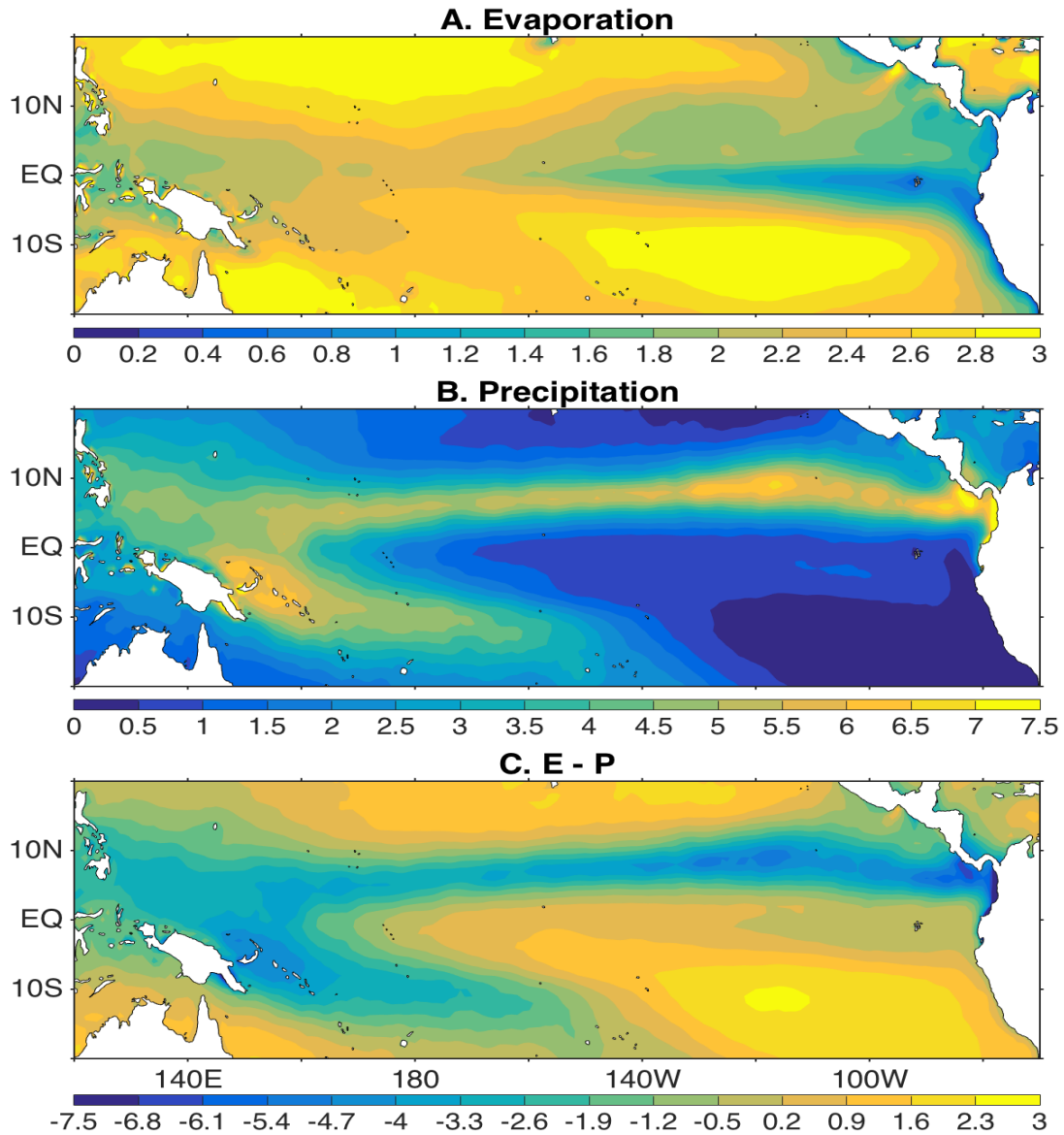
Figure 2.2. Mean (a) evaporation, (b) precipitation, and (c) E–P from monthly ECMWF evaporation and precipitation (mm) for the period from August 2011 to May 2015

18
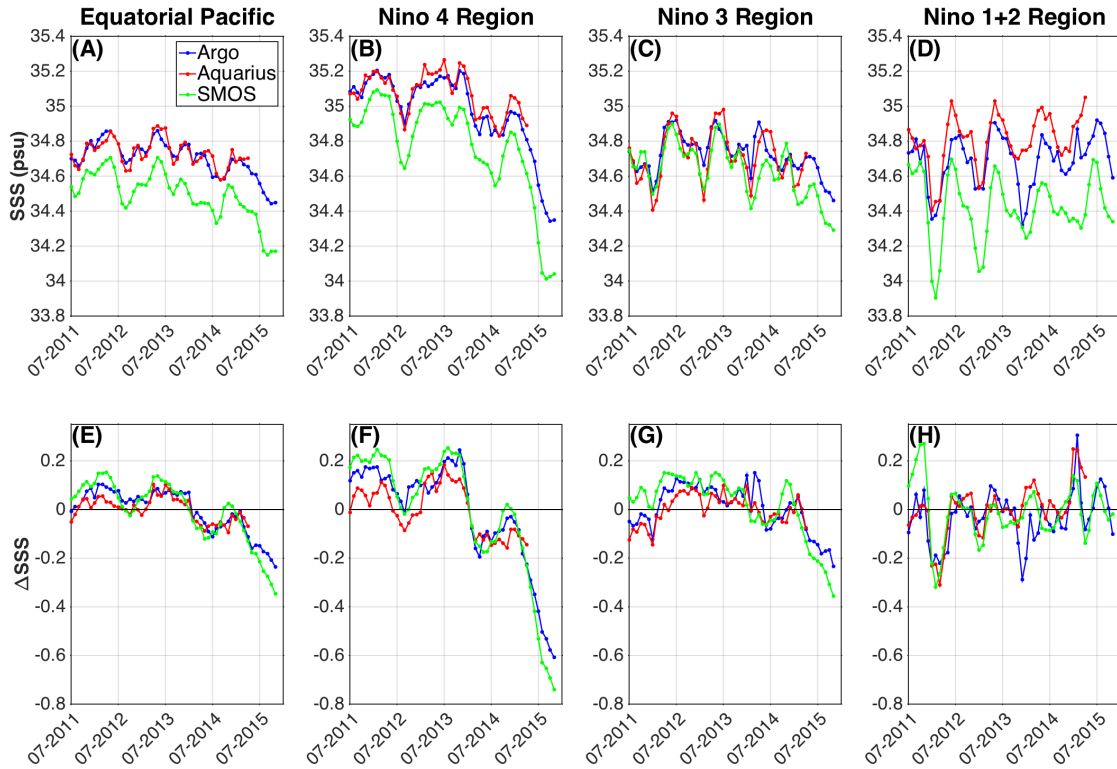
Figure 2.3. (Top Row) SSS variability from Argo (blue), Aquarius (red), and SMOS (green) averaged over (A) equatorial Pacific (5°N-5°S, 130°E-90°W), (B) Niño 4 region (5°N-5°S, 160°E-150°W), (C) Niño 3 region (5°N-5°S, 150°-90°W), and (D) Niño 1 + 2 region (0°-10°S, 90°-80°W). (Bottom Row) monthly SSS anomalies
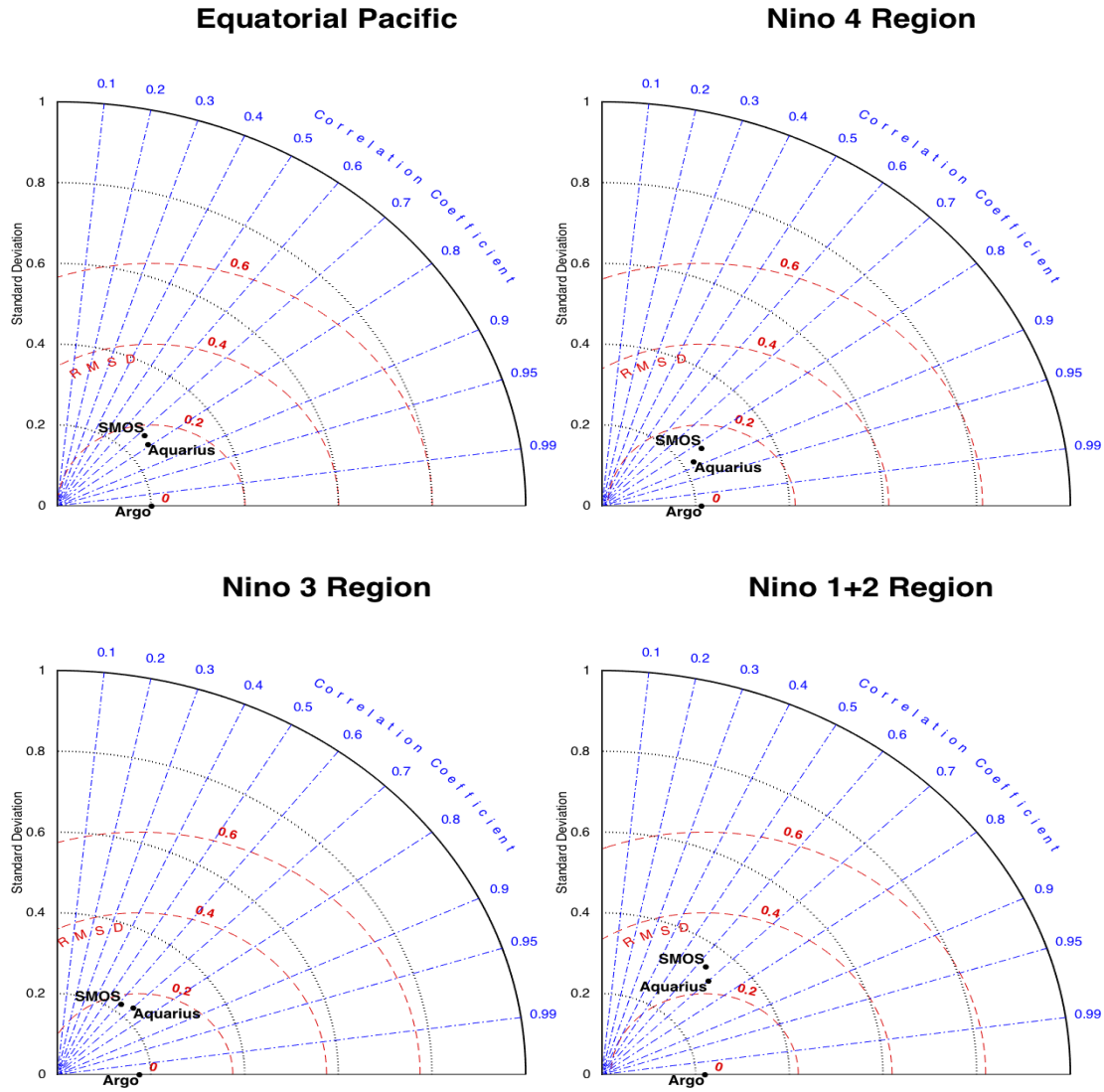
Figure 2.4. Taylor diagrams comparing Aquarius and SMOS SSS anomalies with Argo SSS anomalies with respect to the mean taken from August 2011 to May 2015 in the equatorial Pacific (5°N-5°S, 130°E-90°W), the Niño 4 region (5°N-5°S, 160°E-150°W), the Niño 3 region (5°N-5°S, 150°-90°W) and the Niño 1 + 2 region (0°-10°S, 90°-80°W)

20
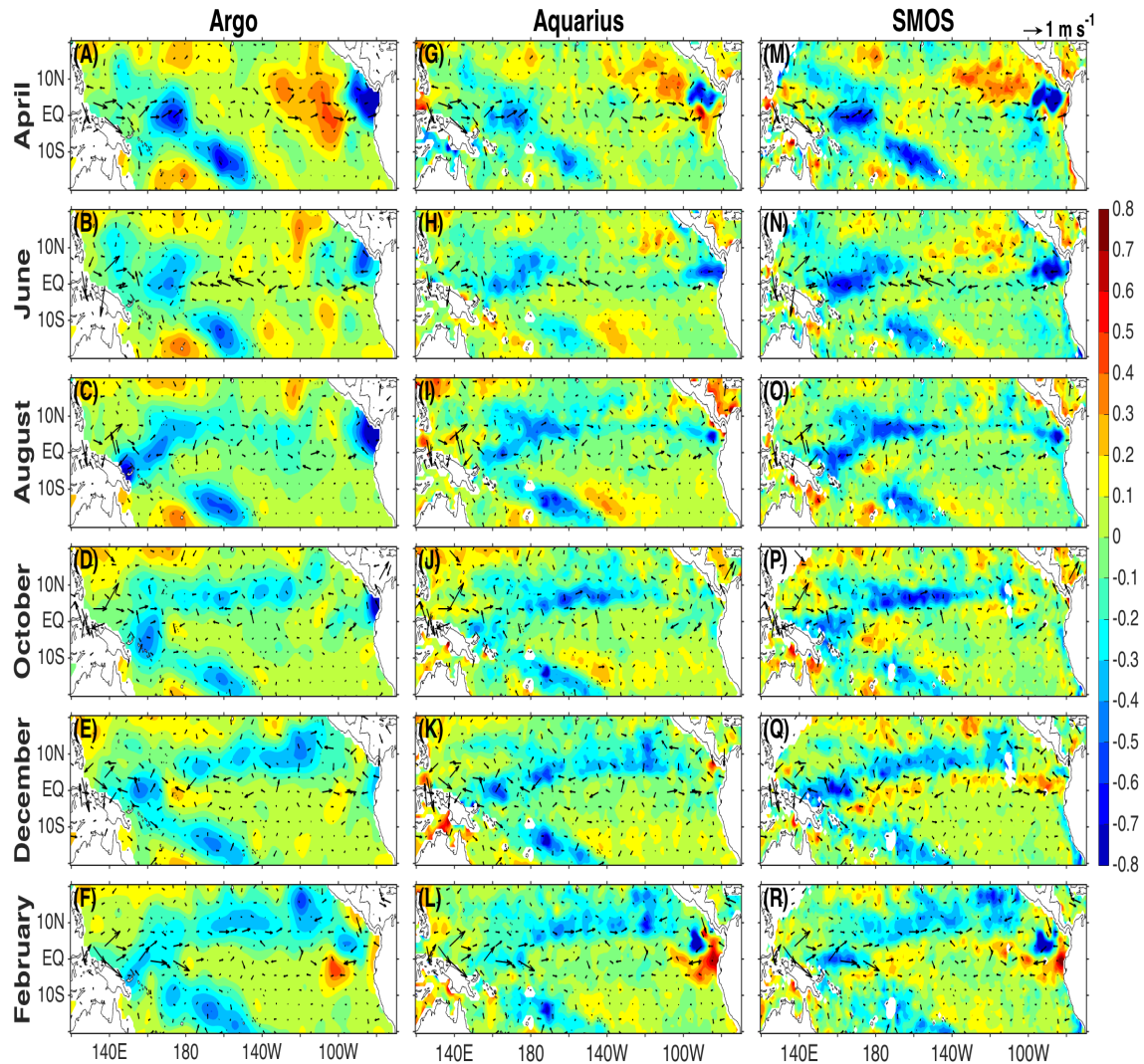
Figure 2.5. SSS anomalies (psu) from April 2014 to February 2015 using Argo (left column), Aquarius (center column), and SMOS (right column). Anomalous OSCAR surface currents (m s^{-1}) for the same month are shown in the black arrows
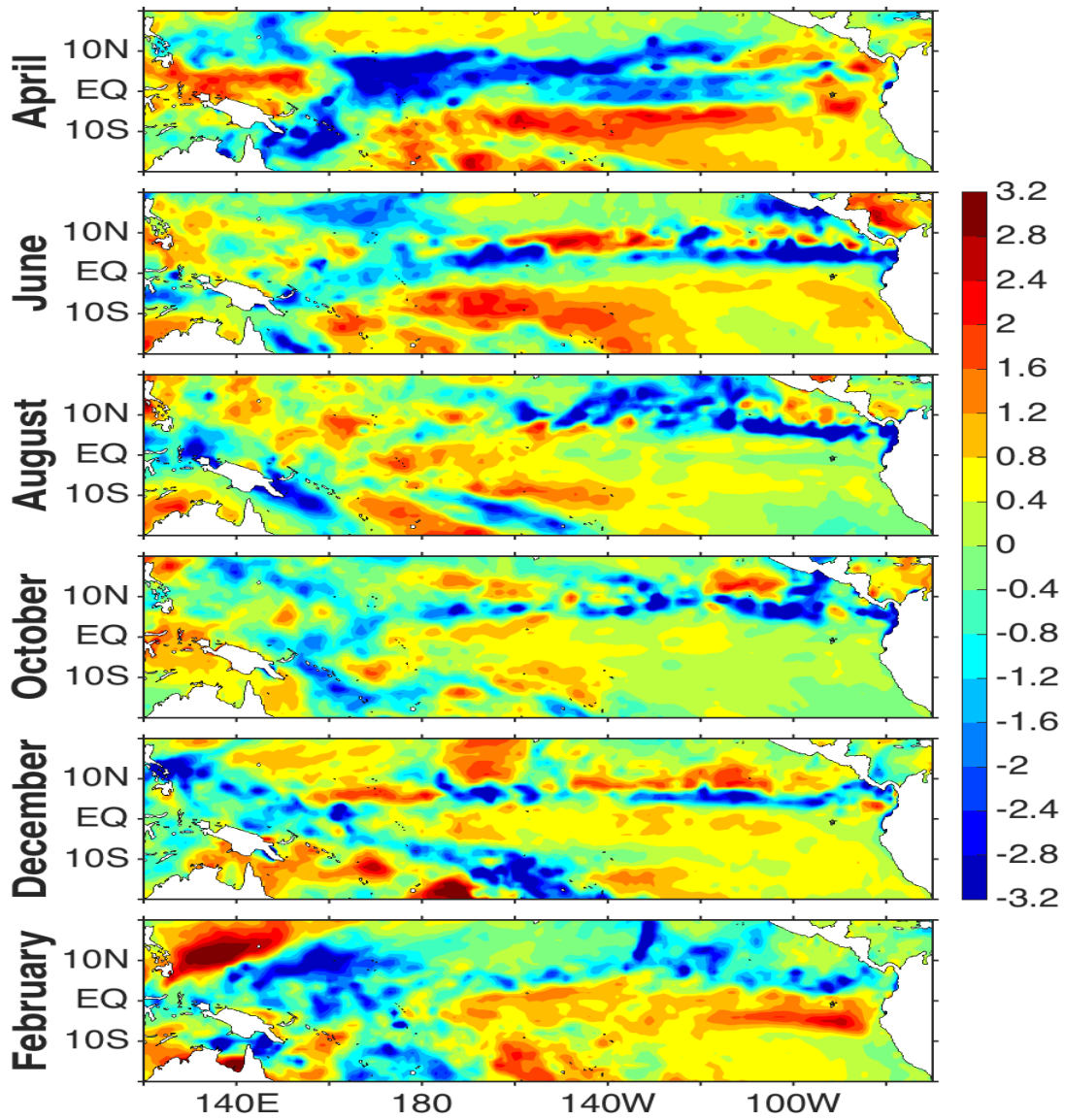
Figure 2.6. Anomalous monthly ECMWF E–P (mm) from April 2014 to February 2015

CHAPTER 3

A COMPARISON OF SEA SURFACE SALINITY IN THE EQUATORIAL PACIFIC

OCEAN DURING THE 1997-98, 2012-13, AND 2014-15 ENSO EVENTS[2]

ABSTRACT

This study examines and compares the sea surface salinity (SSS) variability during the 1997-98 El Niño event and the failed 2012-13 and 2014-15 El Niño events. Our analysis utilizes salinity data from Argo observations and the Simple Ocean Data Assimilation (SODA) reanalysis to examine the SSS variability. Advective processes and evaporation minus precipitation (E-P) variability is understood to influence SSS variability. Using surface wind, surface current, evaporation, and precipitation data, we analyze the causes for the observed SSS variability during each event. This comparison study demonstrates the importance of both advective processes and E-P variability during the generation and onset of a successful El Niño, while a lack of one or both of these processes leads to a failed ENSO event.

3.1 INTRODUCTION

El Niño-Southern Oscillation (ENSO) is an important climatic phenomenon that occurs in the equatorial Pacific Ocean and has local and global implications on weather and biology (Singh et al., 2011; Menkes et al., 2014; Capotondi et al., 2015; McPhaden, 2015). While ENSO involves ocean-atmosphere interactions, it generally includes a zonal displacement of the western Pacific warm pool (Trenberth, 1997; Qu and Yu, 2014). The zonal displacement eastward represents the warm, or positive, phase of ENSO, called El Niño, and the zonal displacement westward represents the cool, or negative, phase of ENSO, called La Niña (Trenberth, 1997; Singh et al., 2011; Qu and Yu, 2014).

24

Conventionally, the phases of ENSO are observed and studied using SST anomalies. Recently, El Niño is being studied by examining sea surface salinity (SSS), surface winds and currents, and sea surface height (SSH) variability (Taft and Kessler, 1991; Li and Clarke, 1994; McPhaden, 1999; Johnson et al., 2000; Menkes et al., 2014).

Lack of extensive and accurate data previously hindered our ability to fully study and understand the connection between SSS variability and ENSO. The Tropical Ocean Global Atmosphere (TOGA)/Tropical Atmosphere Ocean (TOA) mooring project provides in-situ SSS observations across the equatorial Pacific, although the coverage is relatively sparse. SSS data is more readily available with the widespread Argo float network, which has been in operation since 2005. The Simple Ocean Data Assimilation (SODA) reanalysis provides a long-term SSS reanalysis dataset. With long-term and global datasets, SSS data can be examined more thoroughly in connection to El Niño events.

Studying SSS provides a new perspective and an alternative mechanism for viewing and forecasting ENSO. SSS variability during ENSO events has numerous causes and can be influenced by both atmospheric and oceanic dynamics and processes. Advective processes, caused by wind and current variations, and evaporation and precipitation patterns are the two important forcings for SSS variability focused on in this paper.

Westerly Wind Burst (WWB) events, or the slackening and reversal of the Pacific trade winds, affect the direction of surface currents (Menkes et al., 2014). WWB events are highly variable in their duration, but typically last between 5 and 20 days (Harrison and Vecchi, 1997). When WWB events occur, eastward currents dominate the surface

25

current pattern; often, the anomalous surface current pattern lasts longer than the duration of the WWB event (Giese and Harrison, 1990). For the remainder of this paper, it is assumed that anomalously eastward currents are, at least partially, generated by WWB events. Eastward currents throughout the Pacific act to advect the fresh waters of the western Pacific warm pool eastward.

Evaporation and precipitation patterns, specifically E-P, across the Pacific also affect SSS variability. The western Pacific warm pool is characterized by fresh surface waters due to increased convection and precipitation over the region (Delcroix et al., 1996; Chen et al., 2004; Cravatte et al., 2009). Evaporation and precipitation variability is more significant in the eastern Pacific and greatly influences SSS variability in this region (Delcroix et al., 1996). During ENSO changes in the Walker Circulation cause higher than normal precipitation patterns in the western and central Pacific (Lau et al., 1983; Delcroix et al., 1996).

In this study, we compare the 1997-98, 2012-13, and 2014-15 ENSO events to better understand their similarities and differences. Surface winds, surface currents, and evaporation and precipitation patterns are examined to gain a full understanding of their influences on SSS variability during each event. The results of this study aim to advance our understanding of SSS variability during El Niño. We also aim to better characterize the conditions that aided in the development of the 1997-98 El Niño and the conditions that caused the failed development of El Niño in 2012-13 and 2014-15.

26

3.2 MATERIALS AND METHODOLOGY

3.2.1 DATA SOURCES

The International Pacific Research Center (IPRC) processed monthly SSS Argo dataset is available through the Asian Pacific Data Research Center (APDRC). These data are optimally interpolated with a spatial resolution of 1°x1° and available from January 2005 to June 2016. It is important to note that Argo floats measure salinity from 5m to 2,000m depth and this product does not extrapolate the salinity measurement to the surface; therefore the surface salinity measurement used is taken at 5m depth (Moon and Song, 2014; Qu et al., 2014; Song et al., 2015). Lebedev et al., (2007) provides additional information about the methods by which this product is created. SSS anomalies are calculated by removing the monthly means averaged from January 2005 to June 2016.

The Ocean Surface Current Analyses Real-time (OSCAR) uses satellite SSH, wind, and temperature data to estimate zonal and meridional surface currents at a 0.33°x0.33° spatial resolution. The data are output in a 5-day cycle format and available through NASA JPL Physical Oceanography Distributed Active Archive Center (PO.DAAC) from October 1992 to December 2015. For this research, the surface current u- and v- components are averaged for each month and the spatial resolution is reduced to a 1°x1° for comparison with other datasets. Anomalies are calculated by removing the monthly means, which are calculated from October 1992 to December 2015.

The Objectively Analyzed Air-Sea Fluxes (OA Flux) project conducted by the Woods Hole Oceanographic Institution provides monthly ocean evaporation data from January 1958 to September 2015 at a 1°x1° spatial resolution. The data are converted to

27

mm/day and anomalies are calculated by removing the monthly means averaged from January 1958 to September 2015.

NASA Goddard Space Flight Center (GSFC) provides the Tropical Rainfall Measuring Mission (TRMM)-adjusted merged infrared (IR) precipitation data (Product 3B42). Kummerow et al., (1998, 2000) describe the TRMM project and this merged product. The data are available at a 0.25°x0.25° spatial resolution and a 3-hr timescale from January 2000 to August 2015. For comparison with other datasets, the spatial resolution is reduced to 1°x1° and averaged by month. Anomalies are calculated by removing climatology calculated from January 2000 to August 2015.

Global Precipitation Climatology Project (GPCP), provided by NASA GSFC, utilizes data from satellites, rain gauges, and sounding observations to estimate monthly global rainfall totals from January 1979 to October 2015 at a 2.5°x2.5° spatial resolution. Adler et al., (2003) provide a complete explanation of the dataset. For comparison with TRMM, the data are interpolated to a 1°x1° spatial resolution and monthly anomalies are calculated by removing the monthly means from January 1979 to October 2015. This dataset supplements the TRMM data to study years prior to 2000.

3.2.2 REANALYSIS PRODUCTS

The Simple Ocean Data Assimilation (SODA) reanalysis is an ocean reanalysis system. The version 2.2.4 monthly averaged salinity data spans from January 1871 to December 2010 at 0.5°x0.5° spatial resolution. Like Argo, the top-most SODA salinity measurement is at 5m depth. Carton and Giese, (2008) provide a comprehensive description of the SODA reanalysis product, but a brief summary is provided here. This

SODA product is a combination of an ocean model based on the Parallel Ocean Program (POP) and data assimilation (Giese and Ray, 2011). The POP model includes relaxations to climatological SSS on a 3-month timescale. It is important to note that the data assimilation uses salinity profiles obtained through the World Ocean Database, which includes Argo floats. For comparisons with Argo, the spatial resolution is reduced to a 1°x1°. SSS anomalies are calculated by removing the monthly means averaged from January 1950 to December 2010.

The European Centre for Medium-Range Weather Forecasts (ECMWF) ERA-Interim is a global atmospheric reanalysis. For this research, the daily 10 m u-wind component at a 1°x1° spatial resolution are utilized and converted to 5-day averages to study the near-surface zonal winds. The data are available from January 1979 to December 2015.

3.3 RESULTS

3.3.1 WESTERLY WIND BURSTS AND SURFACE CURRENTS

The 1997-98 El Niño is the strongest El Niño event on record (Johnson et al., 2000). Trade winds throughout the equatorial Pacific weakened and reversed in 1997, which pushed warm water from the western Pacific warm pool eastward (McPhaden, 1999). El Niño conditions developed quickly with SST anomalies peaking at values greater than 6°C in the central and eastern Pacific in December 1997 (McPhaden, 1999, 2015). Strong WWB events persisted throughout the summer and winter months of 1997, which maintained the location of the warm SST anomalies in the central and eastern

29

Pacific into the first few months of 1998 (McPhaden, 1999, 2015; Menkes et al., 2014; Picaut et al., 2002).

Frequent and strong WWB events occur at the end of 1996 (Fig. 3.1A). Each event increases in strength and fetch and are more eastwardly located. WWB events continue until November 1997. Winds return to near normal and become anomalously eastward for the remainder of the timeframe. Similar findings are presented by McPhaden, (1999), Picaut et al., (2002), Singh et al., (2011), Fedorov et al., (2015), and Menkes et al., (2014).

Although El Niño conditions were predicted for 2012, they failed to develop (McPhaden, 2015). The onset of El Niño-like conditions occurred later in 2012 than in 1997, but then quickly dissipated. The zonal surface wind pattern lacks strong and frequent WWB events at the end of 2011 and throughout 2012 (Fig. 3.1B). Near normal wind patterns persist in the western Pacific for most of 2011 and 2012. However, numerous small and weak events occur, the strongest of which occurs in early 2012. Compared to 1997, these events are less than half in size and in strength.

Similar to the 2012-13 event, a strong El Niño was predicted in 2014 but failed to develop. This is due to a number of factors, including the lack of sustained eastward winds and currents in the equatorial Pacific (Menkes et al., 2014; McPhaden, 2015). In the early stages of this event, conditions in the equatorial Pacific resemble those observed in early 1997; later, as the El Niño dissipated, conditions more closely resemble the 2012-13 event. This event regenerated into a significant El Niño in mid-2015.

In early 2014, two strong WWB events occur (Fig. 3.1C). These events resemble those in early 1997 in both size and strength. In Spring 2014, winds in the western Pacific

30

become near normal, with a few weak WWB events occurring in the latter half of the year. WWB events occurring throughout 2015 are comparable in size, strength, and location those observed in 1997.

As demonstrated by Fedorov et al., (2015), and others, the WWB events in late 1996 and early 1997 generate anomalously eastward surface currents (Fig. 3.2A). Anomalously eastward currents are initiated by the first two WWB events in late 1996 and early 1997. These currents dominate the equatorial Pacific and continue throughout 1997. After the last WWB event in November, anomalously eastward currents cease and anomalously westward currents persist in 1998.

The surface current anomalies at the end of 2011 are anomalously westward, likely indicating the propagation of westward moving upwelling Rossby waves (Fig. 3.2B). Two short, small and weak eastward current events occur in April 2012 and from August to September 2012. These events co-occur with weak WWB events. This proves the inability for these weak events to initiate strong and long-lasting eastward currents. Interestingly, eastward currents are present in the eastern and central equatorial Pacific from January to July 2012. Weak anomalously westward currents follow the last eastward current event, possibly indicating another Rossby wave pattern.

Strong anomalously eastward currents that stretch across the Pacific are initiated by the two strong WWB events that occur in early 2014 (Fig. 3.2C). Without continuing WWB events, eastward currents cease in the Spring. Some eastward currents remain in the western Pacific for the remainder of 2014, while anomalously westward currents and near normal conditions dominate the central and eastern Pacific. Anomalously eastward

31

currents more similar to those seen in 1997 are initiated when stronger and more frequent WWB events occur in 2015.

3.3.2 SEA SURFACE SALINITY

A small region of weak negative SSS anomalies develops between 130°E and 150°E in late 1996 (Fig. 3.3A). The propagation westward of this region coincides with the earliest WWB events and the initiation of eastward currents. The negative SSS anomalies become fresher cross the International Date Line in March. Negative SSS anomalies continue to propagate into the central and eastern Pacific throughout 1997 and early 1998. The sustained anomalously eastward currents throughout the region in 1997 likely generate the movement of SSS anomalies. Similar findings are presented by McPhaden, (1999), Picaut et al., (2002), Singh et al., (2011), Fedorov et al., (2015), and Menkes et al., (2014). The negative SSS anomalies reach their eastern-most location of 90°W in April 1998, which occurs after eastward currents cease.

Like in 1996, a small region of weak negative SSS anomalies is observed in the western Pacific at the end of 2011 (Fig. 3.3B). However, positive SSS anomalies travelling westward from the International Date Line reach the western Pacific in early 2012 and replace the negative anomalies. This coincides with the anomalously westward currents and Rossby wave pattern. After July 2012, negative SSS anomalies develop at about 170°E; although this co-occurs with the second weak anomalously eastward currents event, there is no eastward propagation of these anomalies. This region then propagates back westward with the return of westward currents.

32

Negative SSS anomalies are located in the western Pacific for much of 2013 (Fig 3.3C). These anomalies begin to move eastward at the end of 2013, before WWB events initiate anomalously eastward currents. The eastern most edge of this region passes the International Date Line before moving back westward and stalling between 150°E and the International Date Line. Additional eastward propagation is likely inhibited by the reversal of surface currents at this time. Eastward propagation of the negative SSS anomalies occurs in mid-2015, signaling the regeneration of the stalled El Niño conditions.

The Niño boxes, shown in Figure 3.4, are previously defined regions for ENSO analysis and forecasting (Trenberth, 1997; Henley et al., 2002). Averaging SSS anomalies in each of the Niño boxes during the 1997-98, 2012-13, and 2014-15 ENSO events provides a timeline for the propagation of negative anomalies across the Pacific.

In 1997, negative SSS anomalies in 1997 are first observed in Niño 4 in April, and a minimum of -0.4psu reached in June (Fig. 3.5A). Anomalies slowly increase during the following months and become positive in September 1998 following the end of the El Niño event. A similar pattern of decreasing anomalies is observed in early 2014 although at a smaller scale. Unlike 1998, anomalies remain negative through the end of 2015. SSS anomalies in 2012 are briefly negative in October 2012, but are otherwise positive.

A similar pattern is observed in Niño 3.4 and Niño 3, with a time delay (Fig. 3.5B, C). In Niño 1+2, 1997-98 SSS anomalies reach two minimums (Fig. 3.5D). The first minimum, of almost -0.9psu, occurs in May and June 1997 and the second minimum, of about -0.5psu, occurs in May 1998. Alternatively, anomalies remain at or near zero for 2012-13 and 2014-15.

Table 3.1 provides a statistical analysis of the data presented in Figure 3.5. For each dataset comparison and in each Niño region, standard deviations are small. RMSDs are also small for each dataset comparison in Niño 4, Niño 3.4 and Niño 3.

In Niño 4, strong positive correlation is found for SODA 97-98 vs. Argo 12-13 and SODA 97-98 vs. Argo 14-15. Removing the final four months of 1998, 2013, and 2014 yields different results. This removes the positive SSS anomalies from the end of 1998. Now, Argo 12-13 is only +51% correlated to SODA 97-98 and Argo 14-15 is +59% correlated to SODA 97-98. This indicates that a slightly stronger correlation exists between Argo 14-15 and SODA 97-98 during El Niño conditions and between Argo 12-13 and SODA 97-98 during the end of El Niño and the onset of La Niña.

The highest correlation between datasets occurs in Niño 3.4 for SODA 97-98 vs. Argo 14-15. SODA 97-98 vs. Argo 12-13 and Argo 12-13 vs. Argo 14-15 are negatively correlated in Niño 3.4 and 3. Compared to the other regions, RMSDs in Niño 1+2 for the SODA vs. Argo comparisons are much larger. Argo 12-13 is moderately and positively correlated to SODA 97-98 in this region.

3.3.3 EVAPORATION AND PRECIPITATION

Negative E-P anomalies are in the western Pacific for much of 1996 (Fig. 3.6A). These anomalies track eastward across the Pacific along a path that is similar to that of the negative SSS anomalies. McPhaden, (1999) and Singh et al., (2011) present similar findings that correspond to the large region of negative E-P anomalies in Figure 3.6A.

Negative E-P anomalies are located in the western Pacific throughout most of 2011, 2012 and 2013 (Fig. 3.6B). Positive E-P anomalies are located at the International

34

Date Line at the end of 2011 and in early 2012; this coincides with the anomalously westward currents, the Rossby wave pattern, and the positive SSS anomalies. Slight eastward propagation of negative E-P anomalies from the western Pacific to the International Date Line occurs in the Spring, and anomalies remain here for the rest of 2012.

Between June and August 2013, significant negative E-P anomalies are observed in the far western Pacific (Fig. 3.6C). Slight eastward propagation of these anomalies is first observed in September 2013. The E-P anomalies follow a track similar to that of the SSS anomalies. It is important to note that eastward currents do not occur during this time. McPhaden, (2015) presents similar findings. While the SSS anomalies stall just west of the International Date Line in mid-2014, negative E-P anomalies propagate back westward. Negative E-P anomalies are again observed propagating eastward with the regeneration of the El Niño in 2015.

Although anomalous E-P is more variable than the SSS anomalies in Niño 4, Niño 3.4 and Niño 3, they follow a similar path (Fig. 3.7A, B, C). It is interesting to note that minimums in E-P anomalies in Niño 3.4 and Niño 3 are reached three months prior to minimums in SSS anomalies. Additionally, near normal and slightly positive E-P anomalies in these regions in the latter half of 1998 are not accompanied by the saltening of SSS.

In Niño 1+2 a large discrepancy between anomalous E-P and SSS occurs in early 1997, when SSS anomalies reach a minimum but E-P anomalies are near zero (Fig. 3.7D). For the second minimum in SSS anomalies in October, E-P anomalies reach a minimum four months prior.

Anomalous E-P and SSS appear to follow similar paths in Niño 4 (Fig. 3.8A). Most notably, a significant drop of SSS anomalies in late 2013 and early 2014 coincides with a drop in E-P anomalies. E-P and SSS anomalies again follow comparable paths in Niño 3.4 until June 2014 (Fig. 3.8B). SSS anomalies reach a minimum in July 2014, while E-P anomalies are near zero. After March 2015, a decrease in E-P anomalies is accompanied by a minor decrease in SSS anomalies. In Niño 3, SSS and E-P anomalies appear to follow similar paths, although there is some variability (Fig. 3.8C). In Niño 1+2, variability in the SSS anomalies cannot be explained by the near zero E-P anomalies (Fig. 3.8D).

Table 3.2 provides correlation coefficients for the data provided in Figure 3.7 and 3.8. E-P and SSS anomalies are highly correlated in Niño 4 and Niño 3.4 during the 1997-98 event. In 2012-13, moderate correlations exit in Niño 4 and Niño 1+2. Minimal or no correlation exists between SSS and E-P anomalies in each of the regions during the 2014-15 event.

3.4 DISCUSSION AND CONCLUSIONS

SSS is an important variable to examine in a comprehensive El Niño analysis. Variability of salinity across the Pacific can be used to track El Niño development. The Niño boxes are important tools to utilize when studying SSS during ENSO, as the longitudinal expanse of negative anomalies is an indicator for the success or failure of an El Niño.

SSS variability in the equatorial Pacific can be caused by a number of factors, including WWB events and E-P patterns. Numerous and strong WWB events trigger

anomalously eastward currents, which act to advect negative SSS anomalies from the western Pacific to the central and eastern Pacific (Menkes et al., 2014). Although E-P variability tends to dominate the SSS pattern more in the eastern Pacific than the central Pacific, changes to the Walker Circulation increase precipitation in the western Pacific during El Niño (Lau et al., 1983; Delcroix et al., 1996; Delcroix and Picaut, 1998).

Frequent and strong WWB events at the end of 1996 and throughout 1997 initiate anomalously eastward surface currents across the Pacific. This allows for the advection of negative SSS anomalies into the central and eastern Pacific. Alternatively, few and weak WWB events occur in 2012 and 2014. These wind events were unable to initiate strong and sustained eastward currents throughout the Pacific, which limits the advection of SSS anomalies.

Anomalously negative E-P tracks along a path similar to the negative SSS anomalies during the 1997-98 El Niño. Statistically, E-P is highly correlated to SSS anomalies in the Niño 4 and Niño 3.4 regions. The two parameters are only highly correlated in the Niño 4 region during the 2012-13. Therefore, E-P processes are important contributors to the SSS variability in the more western Niño regions. Minimal or no correlation exists between the two variables in 2014-15. This likely indicates that advection processes dominate the SSS variability during this event.

Analysis of SSS variability in the Niño regions provides an understanding of the longitudinal expanse of the fresh anomalies. In 1997-98, there is a clear time delay between the arrival of negative SSS anomalies in the Niño 4, 3.4, and 3 regions. A similar pattern occurs during the 2014-15 event. However in 2012-13, negative anomalies are only briefly observed in Niño 4 and are never observed further east. SSS anomalies

37

during 2014-15 and 1997-98 are highly correlated in Niño 4, 3.4, and 3 when excluding the final months of the event. Anomalies during both 1997-98 and 2014-15 are not statistically similar to those in 2012-13.

These results indicate that both advective processes and E-P variability are important and necessary features for the development of El Niño conditions. Without eastward currents to advect negative SSS anomalies across the Pacific, El Niño events cannot fully develop. The collocation of negative SSS and E-P anomalies in addition to the eastward currents are needed for an El Niño to fully develop, as occurred in 1997-98. Absence of one of these factors hinders the ability for El Niño to develop, as happened in 2012-13 and 2014. It is essential that anomalously fresh water pass the International Date Line and move into the central, and, potentially, into the eastern Pacific for El Niño conditions to fully form and sustain long lasting events.

As the Argo float program continues operation, additional studies of SSS in the equatorial Pacific during ENSO events can be conducted to better understand the connection between El Niño onset and the propagation of negative salinity anomalies. Satellite products such as ESA's Soil Moisture Ocean Salinity (SMOS) and NASA's Soil Moisture Active Passive (SMAP) provide continuous global SSS observations at a high resolution. Going forward, these products can be used to conduct near real time analysis of these events as they unfold, and further our understanding of SSS variability during ENSO.

Table 3.1. Comparison of SODA 1997-98 Argo 2012-13, and Argo 2014-15 SSS anomalies (black, blue, and red respectively in Figure 3.5) in each of the Niño boxes

Region	Datasets Compared	Standard Deviation	RMSE	Correlation Coefficient
Niño 4	SODA 97-98 vs. Argo 12-13	0.06	0.12	0.67
	SODA 97-98 vs. Argo 14-15	0.08	0.13	0.54
	Argo 12-13 vs. Argo 14-15	0.08	0.08	0.28
Niño 3.4	SODA 97-98 vs. Argo 12-13	0.04	0.14	-0.38
	SODA 97-98 vs. Argo 14-15	0.06	0.09	0.71
	Argo 12-13 vs. Argo 14-15	0.06	0.09	-0.58
Nino 3	SODA 97-98 vs. Argo 12-13	0.06	0.15	-0.13
	SODA 97-98 vs. Argo 14-15	0.07	0.12	0.39
	Argo 12-13 vs. Argo 14-15	0.07	0.11	-0.43
Nino 1+2	SODA 97-98 vs. Argo 12-13	0.09	0.21	0.53
	SODA 97-98 vs. Argo 14-15	0.09	0.27	-0.16
	Argo 12-13 vs. Argo 14-15	0.09	0.11	0.27

Table 3.2. Correlation coefficients between E-P and SSS anomalies in each of the Niño boxes in 1997-98 (Figure 3.7), 2012-15, 2012-13, and 2014-15 (Figure 3.8)

	Niño 4	Niño 3.4	Niño 3	Niño 1+2
1997-98	0.81	0.60	0.07	-0.01
2012-15	0.58	0.37	0.43	0.27
2012-13	0.61	-0.05	0.39	0.55
2014-15	0.06	0.25	0.35	-0.18

40
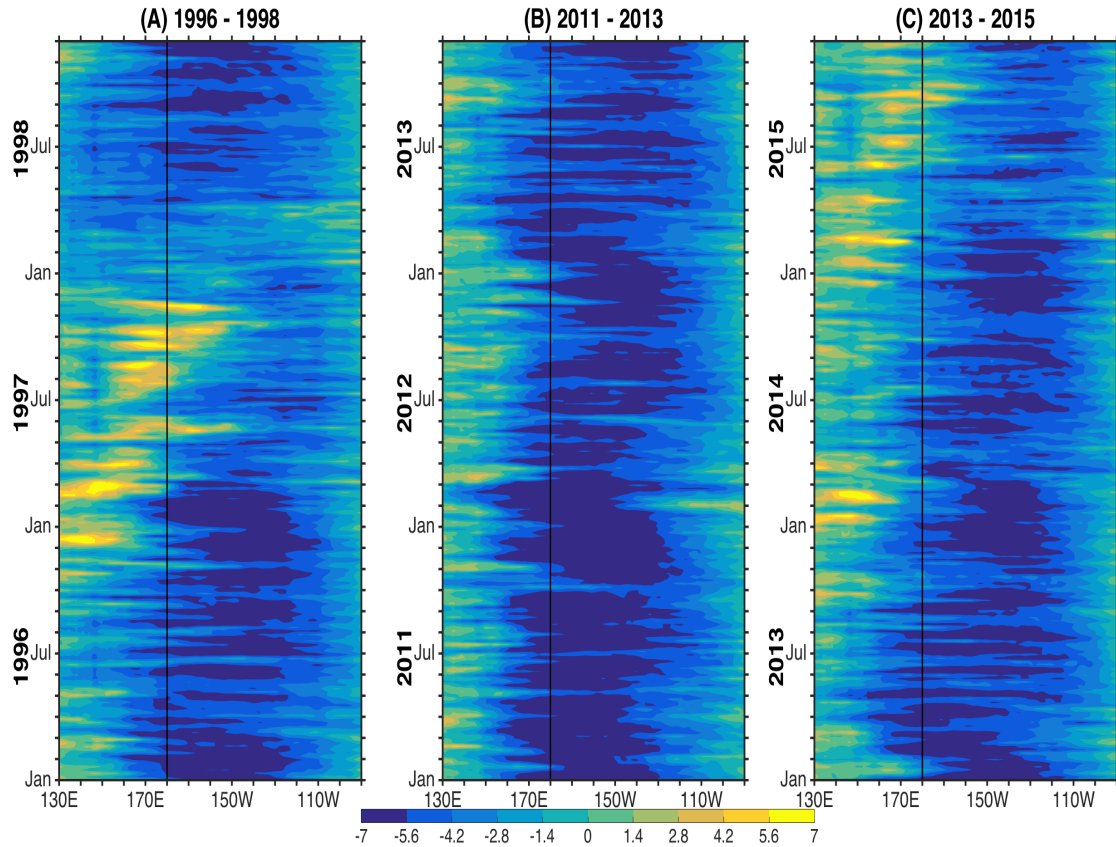
Figure 3.1. Hovmöller diagram from 130°E to 90°W and averaged over 5°N – 5°S of ECMWF 5-day zonal winds (m s^{-1}) for (A) January 1996–December 1998, (B) January 2011–December 2013, and (C) January 2013–December 2015. The black line represents the location of the International Date Line

41
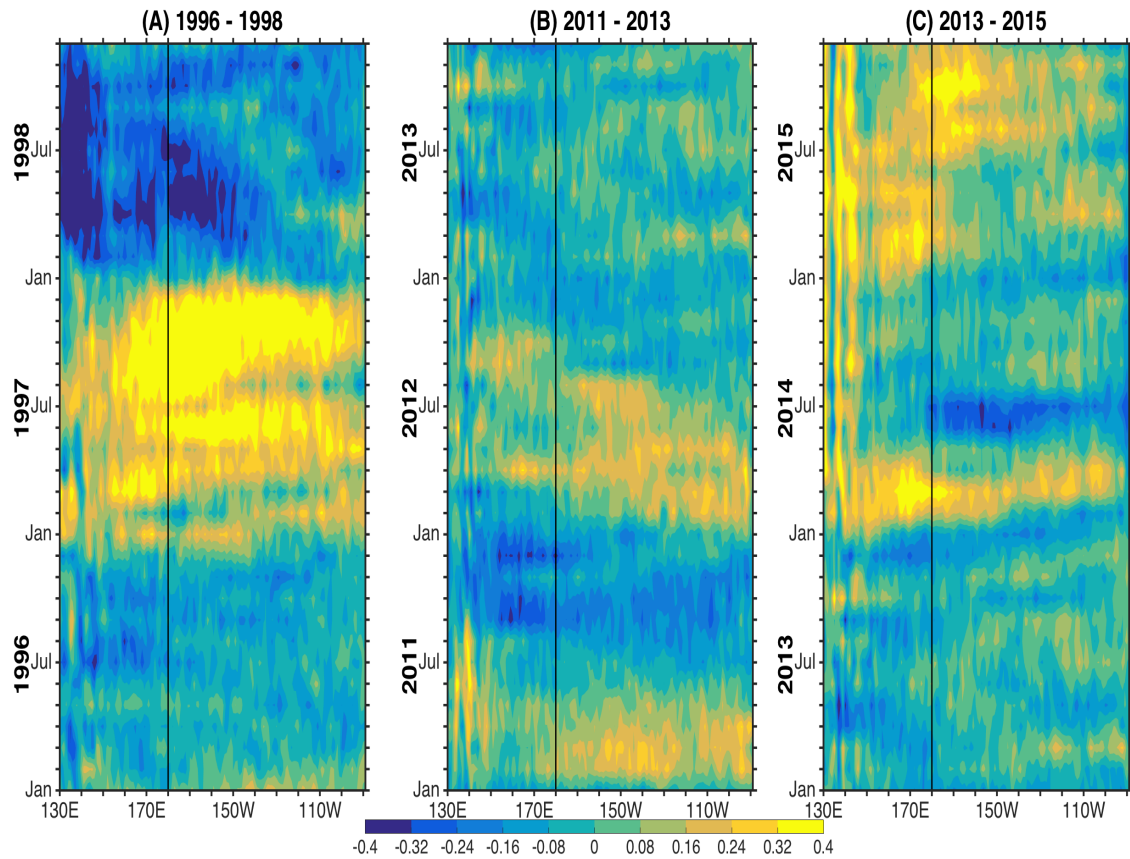
Figure 3.2. Same as Figure 3.1 but for anomalous OSCAR zonal surface currents
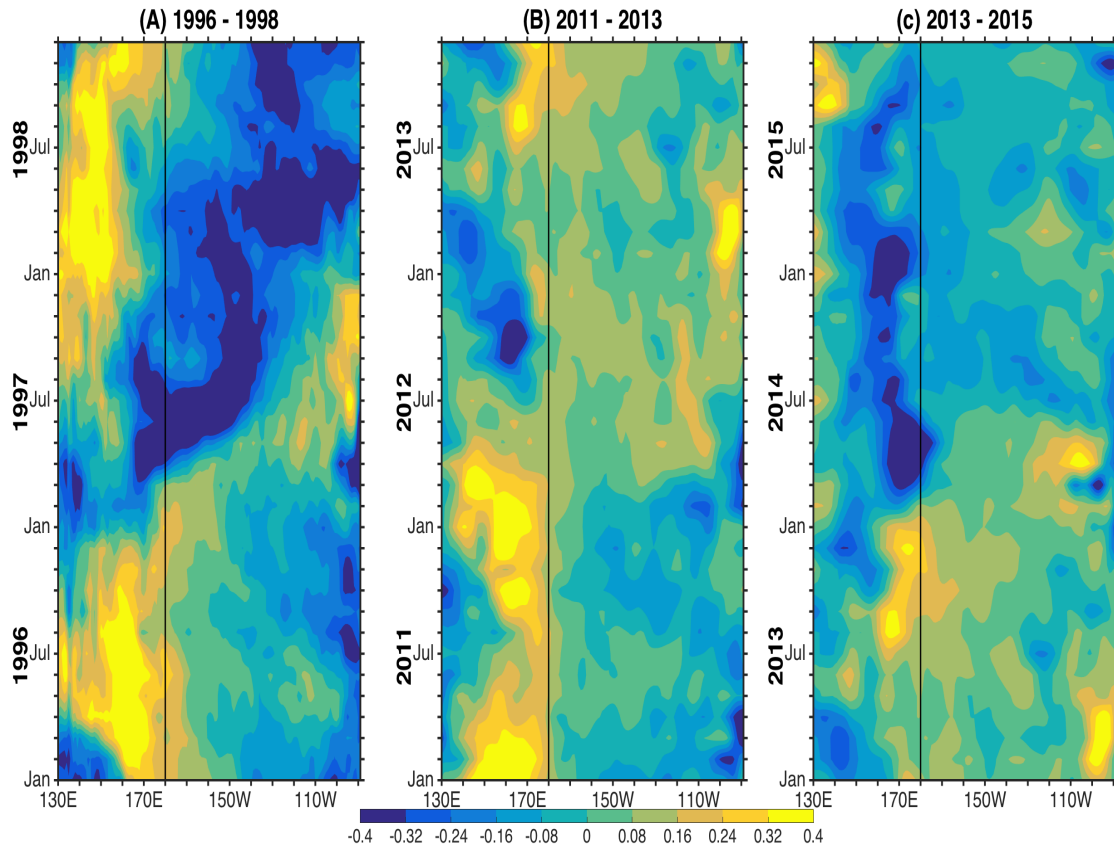
Figure 3.3. Same as Figure 3.1 but for SSS anomalies (psu) using (A) SODA reanalysis and (B, C) Argo
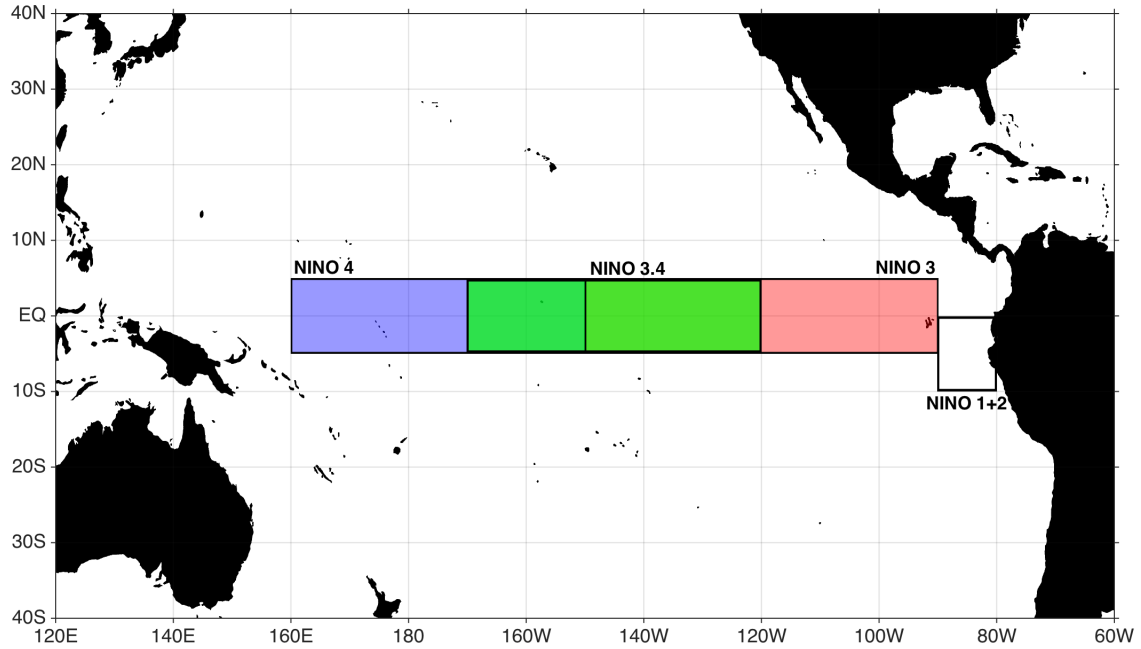
Figure 3.4. Plot of the regions defined as Niño 4, Niño 3.4, Niño 3, and Niño 1+2. Niño 4 is the region from 5°N–5°S, 160°E–150°W (shaded in blue). Niño 3.4 is the region from 5°N–5°S, 170°W–120°W (shaded in green). Niño 3 is the region from 5°N–5°S, 150°W–90°W (shaded in red). Niño 1+2 is the region from 0°–10°S, 90°W–80°W
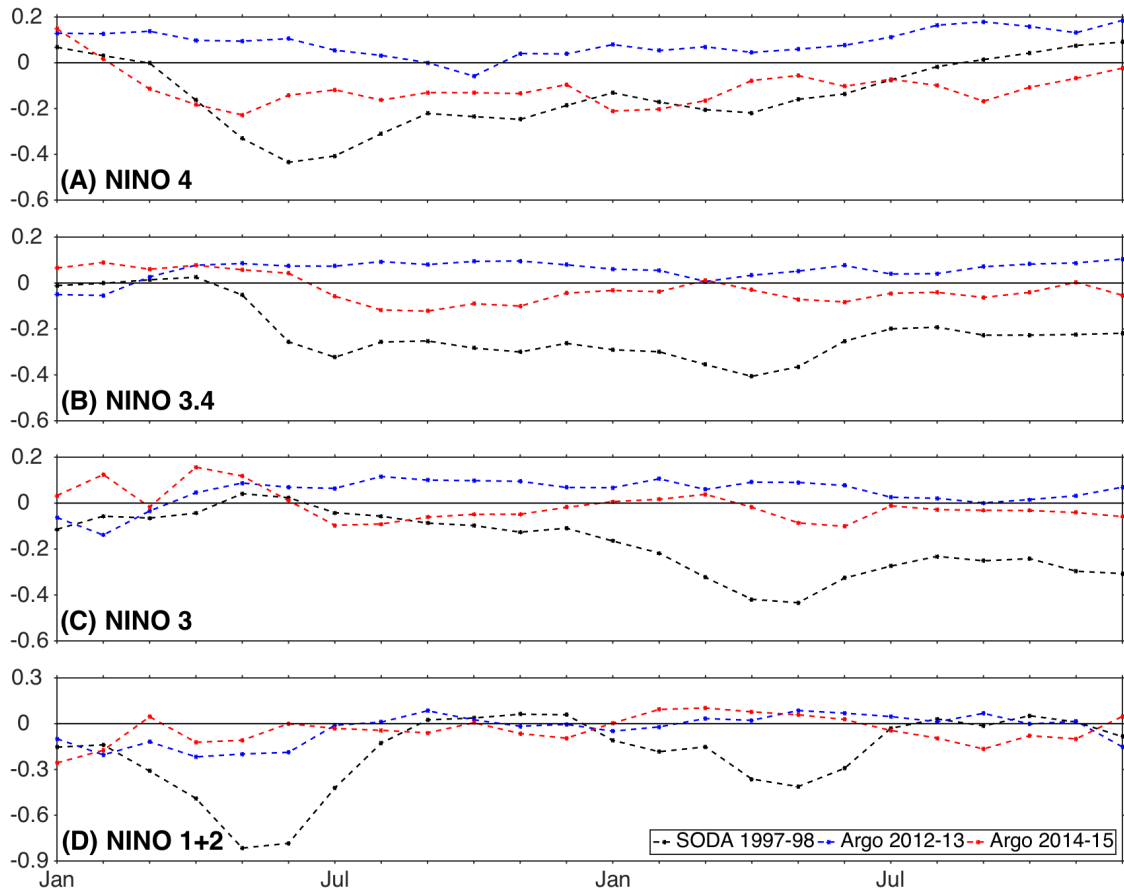
Figure 3.5. Seasonal variability of SSS anomalies (psu) in each of the Niño boxes from SODA (January 1997–December 1998) (black line) and Argo (January 2012–December 2013, January 2014–December 2014) (blue line, red line respectively). Solid black line represents zero
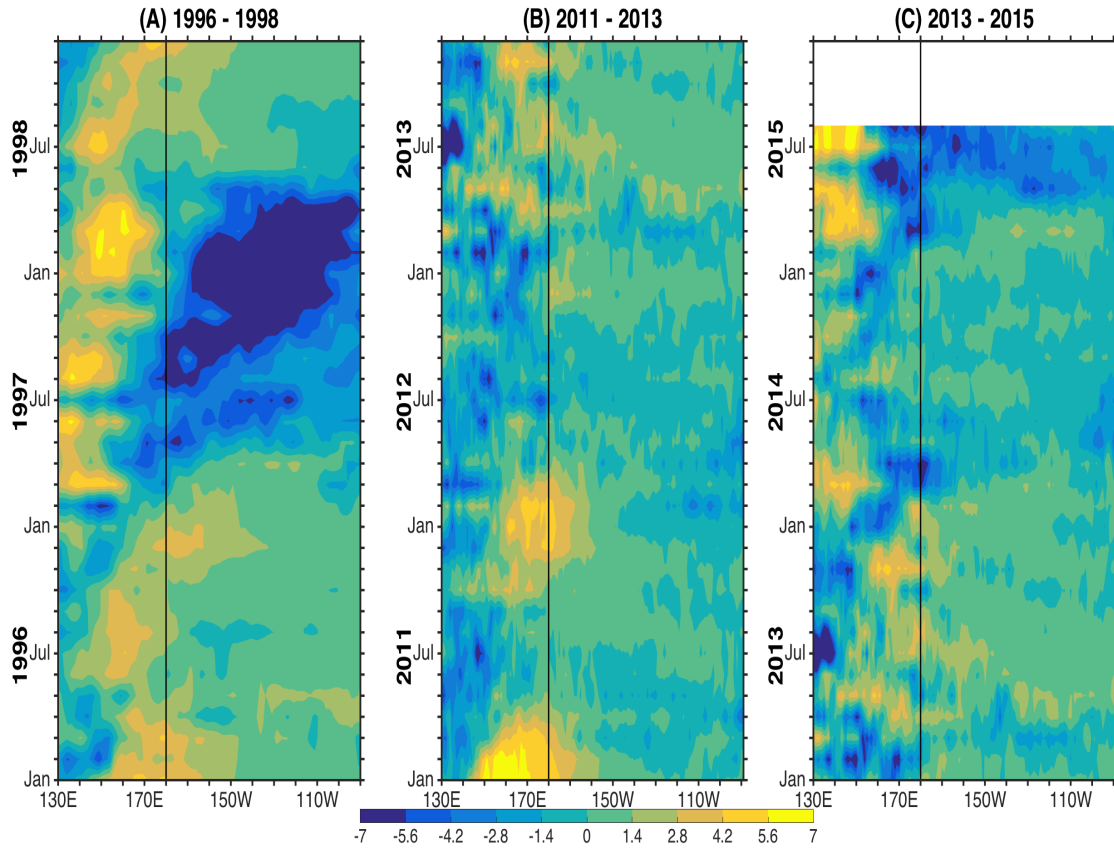
Figure 3.6. Same as Figure 3.1 but for anomalous E–P (mm/day) using OA Flux evaporation and (A) GPCP precipitation, (B, C) TRMM precipitation
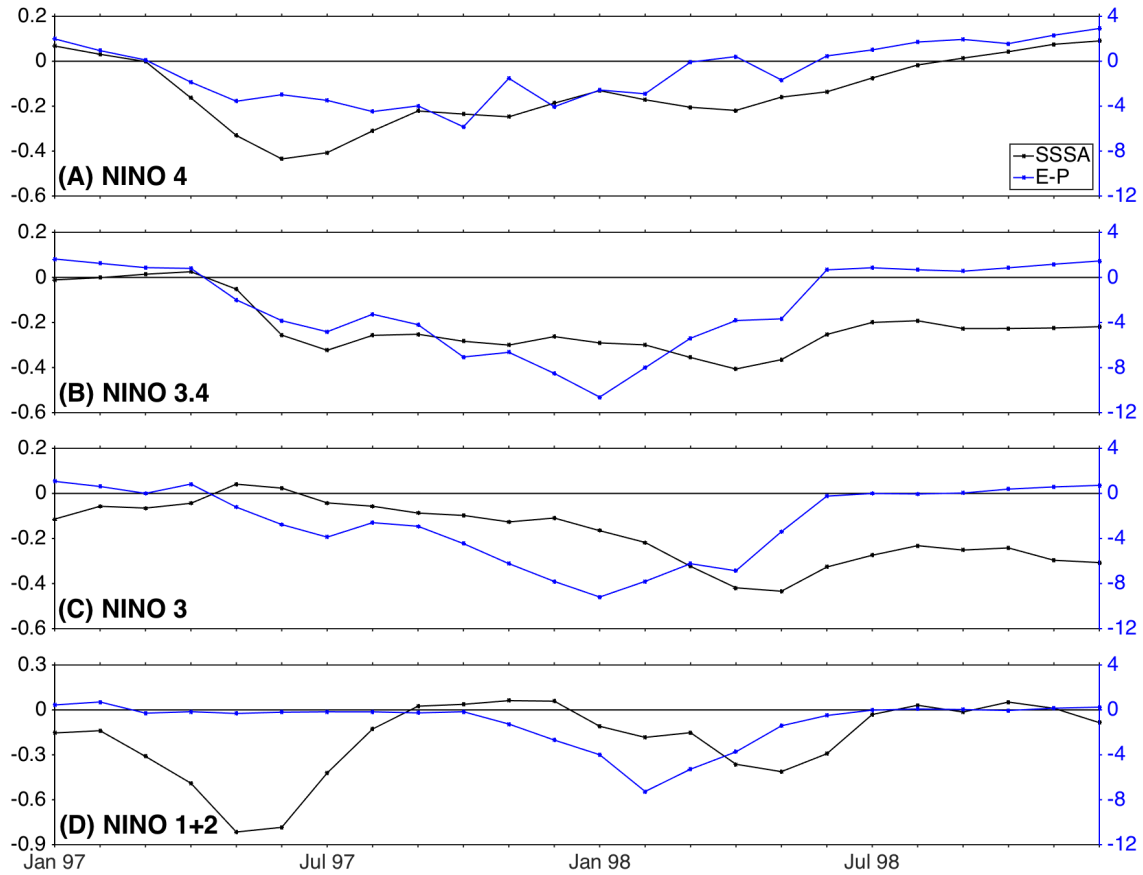
Figure 3.7. Seasonal variability of SODA SSS anomalies (psu) (black line and y-axis) and anomalous E–P (mm/day) using OA Flux evaporation and GPCP precipitation (blue line and y-axis) for each of the Niño boxes from January 1997–December 1998. The black line represents zero
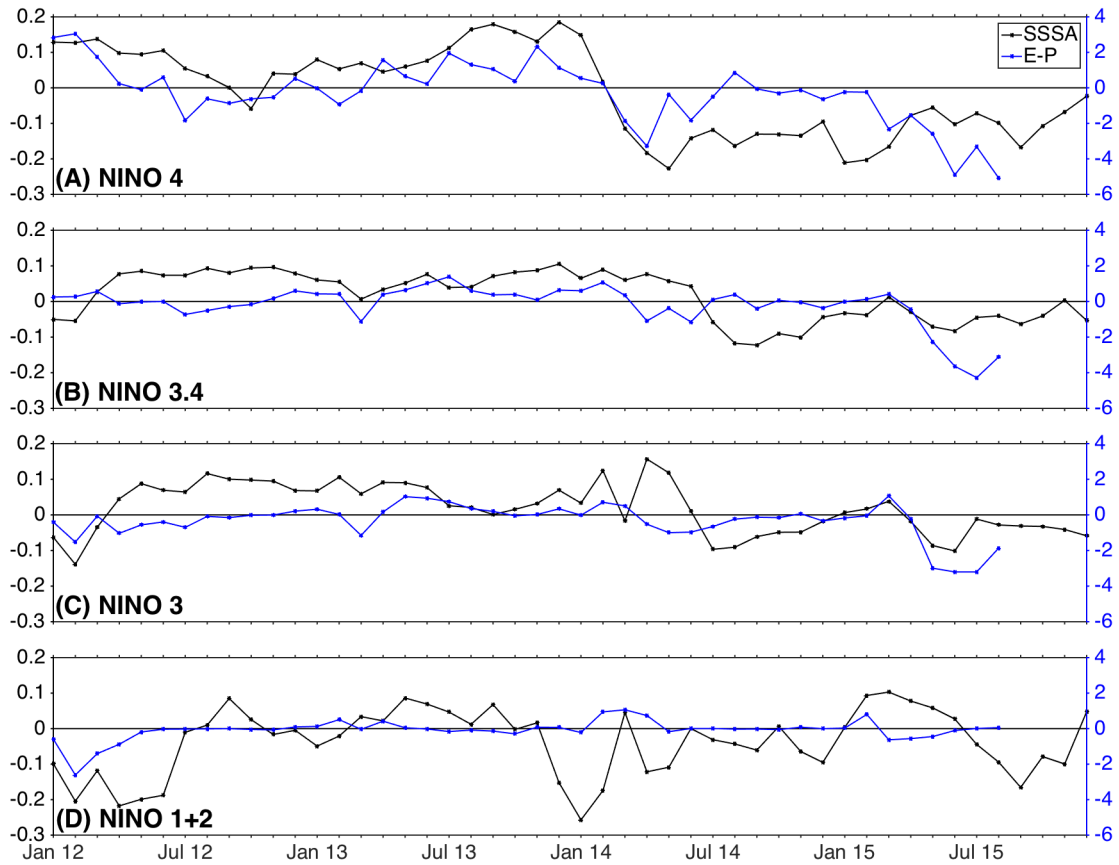
Figure 3.8. Same as Figure 3.7 but for January 2012–December 2015 using Argo SSS anomalies (psu), and anomalous E–P (mm/day) using OA Flux evaporation and TRMM precipitation

CHAPTER 4

CONCLUSIONS

4.1 SUMMARY

This research work focused on SSS variability observed during the phases of ENSO. Previously, SSS changes during ENSO was not well understood and documented. The validity of satellite derived SSS data from Aquarius and SMOS was examined in relation to ENSO studies. Specifically, the failed 2014-15 ENSO event was examined and compared to the 1997-98 El Niño event and the similarly failed 2012-13 ENSO event.

As compared to Argo, the Aquarius and SMOS satellites are capable of resolving SSS variability in the equatorial Pacific. Specifically during the 2014-15 ENSO event, Aquarius, SMOS and Argo are all able to resolve the observed SSS variability. The discrepancies between datasets during this event cannot be fully explained with evaporation and precipitation patterns.

In examining the 2014-15 event more closely, we compared it to the strong 1997-98 El Niño event and the similarly failed 2012-13 ENSO event. This study revealed that both E-P variability and anomalously eastward surface currents are important factors influencing the observed SSS variability. It is determined that both must occur for a successful El Niño to form. Additionally, anomalously fresh SSS must move past the International Date Line during a successful event.

4.2 WESTERN PACIFIC SALINITY INDEX

Using our understanding of SSS during El Niño and using the validated SMOS dataset, we can create climate indices for the prediction of the phases of ENSO. Few salinity indices exist for the prediction of ENSO. Qu and Yu, (2014) developed the Southeastern Pacific SSS Index (SEPSI), which takes the spatial average of SSS in the region from 0° to 10°S and 150°W to 90°W; this region is located just south of Niño 3. Other SSS ENSO indices have been introduced, but they do not incorporate new SSS data available with satellite missions (Delcroix, 1998; Singh et al., 2011; Qu and Yu, 2014). With our findings from Chapter 3, we can identify the International Date Line as an important region that can be used for index development.

We propose a new ENSO index, called the Western Pacific Salinity Index (WPSI), which uses SSS observations in the western and central equatorial Pacific. This location is chosen to capture the maximum variability observed near the International Dateline. The index is calculated using Argo, SMOS, and Aquarius, and is capable of observing El Niño, La Niña and neutral phases of any strength and duration.

WPSI is a 5 month running mean of spatially averaged SSS anomalies in the box from 5°N to 5°S and 160°E to 170°W, shown in blue in Figure 4.1. SSS anomalies of -0.2psu or less for 6 consecutive months, including the month of December, defines an El Niño year. An El Niño year is defined as October through the following September. La Niña is defined as SSS anomalies of +0.2psu or greater. All years that do not meet these criteria are characterized as neutral ENSO.

Since 2005, three El Niño and three La Niña events have occurred (Table 4.1). These events are defined by examining the JMA Index, ONI, and SOI. These three

indices are chosen because their calculation varies significantly. JMA Index is calculated from monthly averaged SSTA in the area between 4°N to 4°S and 150°W to 90°W, known as the Niño 3 region (Trenberth, 1997; Hanley et al., 2002). ONI is a three month running mean of the SST anomalies in the Niño 3.4 region, from 5°N to 5°S and 170°W to 120°W; ONI is also referred to as the Niño 3.4 index (Trenberth, 1997; Trenberth and Stepaniak, 2001; Hanley et al., 2002; Ren and Jin, 2011). SOI is calculated based on the difference in SLP between Darwin, Australia and Tahiti (Trenberth, 1997; Hanley et al., 2002).

Because of their differences in calculation, the three indices do not always agree on the phase of ENSO. For the purposes of this study, at least two indices must agree to define a positive or negative ENSO phase.

Table 4.2 shows the calculation of WPSI using Argo, SMOS and Aquarius. La Niña events are in blue and El Niño events are in red. Argo WPSI captures all but one of the defined events. Like SOI, WPSI with Argo defines 2008-09 as a La Niña year, although JMA and ONI categorize that year as ENSO neutral.

WPSI using SMOS is also successful in identifying the phases of ENSO and matches the consensus categorization displayed in Table 4.1. Argo and SMOS index values are comparable, although they are not always equal. Compared to the Argo calculation, SMOS observes a longer, continuous La Niña event from 2010 to 2012. Aquarius is unable to sense any events. Aquarius WSPI values tend to differ from those of Argo and SMOS by ±0.1psu or more.

When examining a number of established ENSO indices, some variability can be observed (Figure 4.2a). However, the majority of indices tend to agree on the timing of

51

ENSO events. The most significant variability can be observed in the Niño 1+2 index. All indices are highly correlated to each other, 0.8 or greater, except Niño 1+2.

Argo and SMOS values match up well, with only slight differences on the order of less than 0.1psu (Figure 4.2b). Argo and SMOS have a correlation coefficient of 0.97. Aquarius clearly lacks the ability to observe SSS anomalies near the extremes, as evident in 2013 and 2015. This makes Aquarius an ineffective tool for the calculation of WPSI.

Contrasting the indices in Figure 4.2a, WPSI values are negative during El Niño and positive during La Niña. WPSI using Argo and SMOS are highly, and negatively, correlated to all indices in Figure 4.2a, except Niño 1+2. Correlation coefficients for the WPSI calculations compared to the indices are -0.8 or greater. For Niño 1+2, correlation coefficients are -0.43 and -0.60 for Argo WPSI and SMOS WPSI respectively.

This work can be developed further and new SSS tools can be implemented. In June 2015, the Aquarius mission ended, which limits the available SSS data. NASA's Soil Moisture Active Passive (SMAP) satellite, which launched in January 2015, was originally intended to only observe soil moisture; with the end of Aquarius, SMAP has been adapted to also retrieve SSS data. As both SMAP and SMOS continue to collect salinity measurements, we can further develop long-term global high-resolution SSS data and implement said data into climate indices and ENSO studies.

Table 4.1. Phases of ENSO from 2005 to 2016 as defined by Japan Meteorological Agency Index (JMA), Oceanic Niño Index (ONI) and the Niño 3.4 Index

	JMA	ONI	SOI
2005 - 2006	Neutral	Neutral	Neutral
2006 - 2007	El Niño	El Niño	Neutral
2007 - 2008	La Niña	La Niña	La Niña
2008 - 2009	Neutral	Neutral	La Niña
2009 - 2010	El Niño	El Niño	El Niño
2010 - 2011	La Niña	La Niña	La Niña
2011 - 2012	Neutral	La Niña	La Niña
2012 - 2013	Neutral	Neutral	Neutral
2013 - 2014	Neutral	Neutral	Neutral
2014 - 2015	El Niño	Neutral	Neutral
2015 - 2016	El Niño	El Niño	El Niño

Table 4.2. Proposed WPSI values calculated using (A) Argo, (B) SMOS, and (C) Aquarius. Following the criteria, El Niño events are colored red and La Niña events are colored blue

(A) ARGO

	Jan	Feb	Mar	Apr	May	Jun	Jul	Aug	Sep	Oct	Nov	Dec
2005	-	-	-	-	-0.14	-0.11	-0.08	-0.06	-0.07	-0.07	-0.05	-0.02
2006	0.03	0.09	0.11	0.12	0.11	0.08	0.00	-0.07	-0.15	-0.23	-0.31	-0.37
2007	-0.38	-0.33	-0.26	-0.17	-0.09	-0.03	0.00	0.03	0.08	0.15	0.21	0.25
2008	0.27	0.27	0.26	0.23	0.21	0.19	0.17	0.16	0.18	0.21	0.26	0.30
2009	0.33	0.35	0.34	0.31	0.27	0.22	0.15	0.06	-0.02	-0.11	-0.19	-0.29
2010	-0.36	-0.39	-0.39	-0.34	-0.24	-0.11	-0.01	0.10	0.19	0.25	0.29	0.32
2011	0.32	0.31	0.29	0.26	0.24	0.21	0.19	0.17	0.18	0.20	0.20	0.23
2012	0.25	0.26	0.25	0.25	0.22	0.21	0.17	0.13	0.09	0.03	0.00	0.00
2013	0.01	0.04	0.09	0.10	0.11	0.11	0.12	0.14	0.18	0.20	0.21	0.24
2014	0.23	0.19	0.11	0.02	-0.11	-0.19	-0.22	-0.23	-0.19	-0.14	-0.12	-0.11
2015	-0.09	-0.08	-0.09	-0.12	-0.17	-0.24	-0.29	-0.35	-0.40	-0.45	-0.49	-0.54
2016	-0.57	-0.59	-0.59	-0.50	-0.41	-0.33	-	-	-	-	-	-

(B) SMOS

	Jan	Feb	Mar	Apr	May	Jun	Jul	Aug	Sep	Oct	Nov	Dec
2010	-	-	-	-	0.17	0.18	0.19	0.21	0.25	0.30	0.35	0.38
2011	0.39	0.37	0.34	0.32	0.30	0.28	0.26	0.23	0.23	0.23	0.22	0.23
2012	0.24	0.25	0.26	0.26	0.26	0.26	0.22	0.16	0.09	0.01	-0.06	-0.08
2013	-0.08	-0.05	0.01	0.07	0.12	0.15	0.18	0.19	0.21	0.22	0.23	0.23
2014	0.20	0.14	0.06	-0.03	-0.13	-0.20	-0.24	-0.24	-0.21	-0.18	-0.13	-0.09
2015	-0.07	-0.06	-0.07	-0.11	-0.17	-0.23	-0.30	-0.38	-0.46	-0.54	-0.60	-0.66
2016	-0.69	-0.70	-0.68	-0.63	-0.55	-0.43	-	-	-	-	-	-

(C) AQUARIUS

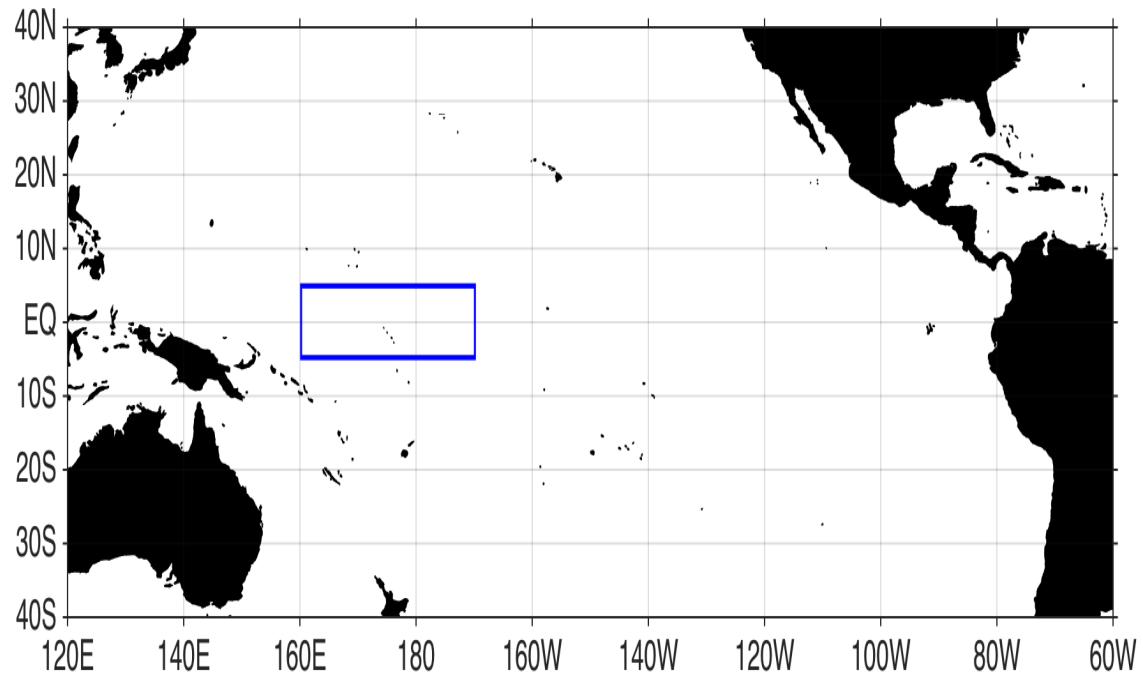|	Jan	Feb	Mar	Apr	May	Jun	Jul	Aug	Sep	Oct	Nov	Dec
2011	-	-	-	-	-	-	-	-	-	-	-	0.12
2012	0.13	0.15	0.15	0.16	0.16	0.16	0.12	0.08	0.02	-0.05	-0.09	-0.11
2013	-0.10	-0.09	-0.03	0.04	0.10	0.12	0.16	0.17	0.16	0.14	0.15	0.15
2014	0.12	0.08	0.03	-0.04	-0.10	-0.16	-0.18	-0.18	-0.16	-0.16	-0.15	-0.16
2015	-0.15	-0.15	-0.15	-0.15	-0.15	-	-	-	-	-	-	-

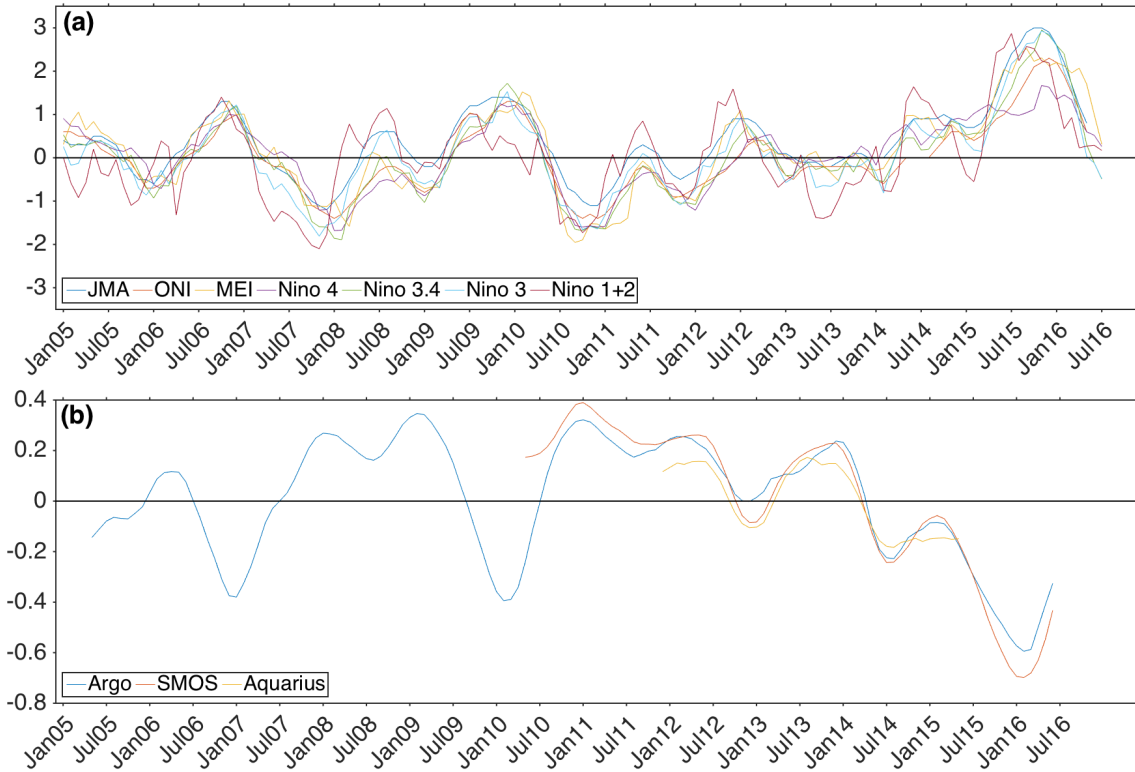Figure 4.1. Proposed WPSI box from 5°N to 5°S and 160°E to 170°W

Figure 4.2. Time series from January 2005 to December 2016 of (a) JMA, ONI, MEI, Niño 4, Niño 3.4, Niño 3, Niño 1+2 indices and (b) proposed WPSI using Argo, SMOS, and Aquarius

56

REFERENCES

Adler, R. F., G. J. Huffman, A. Chang, R. Ferraro, P. P. Xie, J. Janowiak, B. Rudolf, U. Schneider, S. Curtis, D. Bolvin, A. Gruber, J. Susskin, P. Arkin, and E. Nelkin. 2003. The version-2 Global Precipitation Climatology Project (GPCP) monthly precipitation analysis (1979-Present). *J. Hydrometeor*. 4: 1147-1167. doi: 10.1175/1525-7541(2003)004<1147:TVGPCP>2.0.CO;2

Bingham, F. M., G. R. Foltz, and M. J. McPhaden. 2012. Characteristics of the seasonal cycle of surface layer salinity in the global ocean. *Ocean Sci*. 8 (5): 915-929. doi: 10.5194/osd-8-2377-2011.

Boutin, J., N. Martin, N. Kolodziejczyk, and G. Reverdin. 2016. Interannual anomalies of SMOS sea surface salinity. *Rem. Sens. Envir*. 180: 128-136. doi: 10.1016/j.rse.2016.02.053.

Boutin, J., N. Martin, G. Reverdin, X. Yin, and F. Gaillard. 2013. Sea surface freshening from SMOS and ARGO salinity: Impact of rain. *Ocean Sci*. 9: 183-192. doi: 10.5194/osd-9-3331-2012.

Capotondi, A., A. T. Wittenberg, M. Newman, E. Di Lorenzo, J. Y. Yu, P. Braconnot, J. Cole, B. Dewitte, B. Giese, E. Guilyardi, F. F. Jin, K. Karnauskas, B. Kirtman, T. Lee, N. Schneider, Y. Xue, and S. W. Yeh. 2015. Understanding ENSO diversity. *Bull. Am. Meteorol. Soc*. 96: 921–938. doi: 10.1175/BAMS-D-13-00117.1.

Carton, J. A., and B. S. Giese. 2008. A reanalysis of ocean climate using Simple Ocean Data Assimilation (SODA). *Mon. Wea. Rev*. 136: 2999-3017. doi: 10.1175/2007MWR1978.1.

Chavez, F. P., P. G. Strutton, G. E. Friederich, R. A. Feely, G. C. Feldman, D. G. Foley, and M. J. McPhaden. 1999. Biological and Chemical Response of the Equatorial Pacific Ocean to the 1997-98 El Niño. *Science* 286: 2126-2131. doi: 10.1126/science.286.5447.2126

Chen, G., C. Fang, C. Zhang, and Y. Chen. 2004. Observing coupling effects between warm pool and "rain pool" in the Pacific Ocean. *Rem. Sens. Environ*. 91: 153-159. doi: 10.1016/j.rse.2004.02.010.

Cravatte, S., T. Delcroix, D. Zhang, M. McPhaden, and J. Leloup. 2009. Observed freshening and warming of the western Pacific warm pool. *Clim. Dyn*. 33: 565-589. doi: 10.1007/s00382-009-0526-7.

Delcroix, T., C. Henin, V. Porte, and P. Arkin. 1996. Precipitation and sea surface salinity in the tropical Pacific Ocean. *Deep Sea Res. Part I Oceanogr. Res. Pap*. 43 (7): 1123-1141. doi: 10.1016/0967-0637(96)00048-9.

Delcroix, T., and J. Picaut. 1998. Zonal displacement of the western equatorial Pacific "fresh pool". *J. Geophys. Res*. 103: 1087-1098. doi: 10.1029/97JC1912.

Fedorov, A. V., H. Shineng, M. Lengaigne, and E. Guilyardi. 2015. The impact of westerly wind bursts and ocean initial state on the development, and diversity of El Niño events. *Clim. Dyn.* 44: 1381-1401. doi: 10.1007/s00382-014-2126-4.

58

Foltz, G. R., and M. J. McPhaden. 2008. Seasonal mixed layer salinity balance of the tropical North Atlantic Ocean. *J. Geophys. Res.* 113: C02013. doi: 10.1029/2007JC004178.

Giese, B. S., and D. E. Harrison. 1990. Aspects of the Kelvin wave response to episodic wind forcing. *J. Geophys. Res.* 95 (C5): 7289–7312. doi: 10.1029/JC095iC05p07289.

Giese, B. S., and S. Ray. 2011. El Niño variability in simple ocean data assimilation (SODA), 1871-2008. *J. Geophys. Res.* 116: C02024. doi: 10.1029/2010JC006695.

Hanley, D. E., M. A. Bourassa, J. J. O'Brien, S. R. Smith, and E. R. Spade. 2002. A quantitative evaluation of ENSO indices. *J. Clim.* 16: 1249-1258. doi: 10.1175/1520-0442(2003)16<1249:AQEOEI>2.0.CO;2.

Harrison, D. E., and G. A. Vecchi. 1997. Surface westerly wind events in the tropical Pacific 1986-1995. *J. Clim.* 10: 3131-3156. doi: 10.1175/1520-0442(1997)010<3131:WWEITT>2.0.CO;2.

Hasson, A., T. Delcroix, J. Boutin, R. Dussin, and J. Ballabrera-Poy. 2014. Analyzing the 2010-2011 La Niña signature in the tropical Pacific sea surface salinity using in situ data, SMOS observations, and a numerical simulation. *J. Geophys. Res.* 119: 3855-3867. doi: 10.1002/2013JC009388.

Henocq, C., J. Boutin, G. Reverdin, F. Petitcolin, S. Arnault, and P. Lattes. 2010. Vertical variability of near-surface salinity in the tropics: Consequences for L-ban radiometer calibration and validation. *J. Atmos. Ocean Tecnol.* 27: 192-209. doi: 10.1175/2009JTECHO670.1.

Johnson, G. C., M. J. McPhaden, G. D. Rowe, and K. E. McTaggart. 2000. Upper equatorial Pacific Ocean current and salinity variability during the 1996-1998 El Niño-La Niña cycle. *J. Geophys. Res.* 105: 1037-1053. doi: 10.1029/1999JC900280.

Kummerow, C., W. Barnes, T. Kozu, J. Shiue, and J. Simpson. 1998. The Tropical Rainfall Measuring Mission (TRMM) sensor package. *J. Atmos. Oceanic Technol.* 15: 809-817. doi: 10.1175/1520-0426(1998)015<0809:TTRMMT>2.0.CO;2.

Kummerow, C., J. Simpson, O. Thiele, W. Barnes, A. T. C. Chang, E. Stocker, R. F. Adler, A. Hou, R. Kakar, F. Wentz, P. Ashcroft, T. Kozu, Y. Hong, K. Okamoto, T. Iguchi, H. Kuroiwa, E. Im, Z. Haddad, G. Huffman, B. Ferrier, W. S. Olson, E. Zipser, E. A. Smith, T. T. Wilheit, G. North, T. Krishnamurti, and K. Nakamura. 2000. The status of the Tropical Rainfall Measuring Mission (TRMM) after two years in orbit. *J. Appl. Meteor.* 39: 1965-1982. doi: 10.1175/1520-0450(2001)040<1965:TSOTTR>2.0.CO;2.

Lagerloef, G., R. R. Colomb, D. Le Vine, F. Wentz, S. Yueh, C. Rug, J. Lilly, J. Gunn, Y. Chao, A. deCharon, and G. Feldman. 2008. Aquarius/SAC-D mission: Designed to meet the salinity remote-sending challenge. *Oceanography* 21: 68-81. doi: 10.5670/oceanog.2008.68.

Lau, K. M., and P. H. Chan. 1983. Short-term climate variability and atmospheric teleconnections from satellite observed outgoing longwave radiation. Part I: Simultaneous relationships. *J. Atmos. Sci.* 40: 2735-2750. doi: 10.1175/1520-0469(1983)040<2735:STCVAA>2.0.CO;2.

Lebedev, K. V., H. Yoshinari, N. A. Maximenko, and P. W. Hacker. 2007. YoMaHa'07: Velocity data assessed from trajectories of Argo floats at parking level and at the sea surface. *IPRC Technical Note* 4(2).

Li, B., and A. J. Clarke. 1994. An examination of some ENSO mechanisms using interannual sea level at the eastern and western equatorial boundaries and the zonally averaged equatorial wind. *J. Phys. Oceanogr.* 24: 681-690. doi: 10.1175/1520-0485(1994)024<0681:AEOSEM>2.0.CO;2.

Maes, C., N. Peul, D. Behringer, and T. O. Kane. 2014. The salinity signature of he equatorial Pacific cold tongue as revealed b the satellite SMOS mission. *Geosci. Lett.* 1: 1-7. doi: 10.1186/s40562-014-0017-5.

Maes, C., J. Picaut, and S. Belamari. 2002. Salinity barrier layer and onset of El Niño in a Pacific coupled model. *J. Geophys. Res. Lett.* 29 (24): 59-1–59-4. doi: 10.1029/2002GL016029.

Maes, C., J. Picaut, and S. Belamari. 2004. Importance of the salinity barrier layer for the buildup of El Niño. *J. Clim.* 18: 104-118. doi: 10.1175/JCLI-3214.1.

McPhaden, M. J. 1999. Genesis and evolution of the 1997-98 El Niño. *Science* 283 (5404): 950-954. doi: 10.1126/science.283.5404.950.

McPhaden, M. J. 2015. Playing hide and seek with El Niño. *Nat. Clim. Change* 5: 791-795. doi: 10.1038/nclimate2775.

Menkes, C. E., M. Lengaigne, J. Vialard, M. Puy, P. Marchesiello, S. Cravatte, and G. Cambon. 2014. About the role of Westerly Wind Events in the possible development of an El Niño in 2014. Geophys. Res. Lett. 41 (18): 6476-6483. doi: 10.1002/2014GL061186.

Moon, J. H., and Y. T. Song. 2014. Seasonal salinity stratifications in the near-surface layer from Aquarius, Argo, and an ocean model: Focusing on the tropical Atlantic/Indian Oceans. J. Geophys. Res Oceans 119: 6066-6077. doi: 10.1002/2014JC009969.

Nyadjro, E. S., and B. Subrahmanyam. 2014. SMOS mission reveals the salinity structure of the Indian Ocean Dipole. *IEEE Geosci. Remote Sens. Lett*. 11 (9): 1564-1568. doi: 10.1109/LGRS.2014.2301594.

Olmedo E., J. Martinez, M. Umbert, N. Hoareau, M. Portabella, J. Ballabrera-Poy, and A. Turiel. 2016. Improving time and space resolution of SMOS salinity maps using multifractal fusion. *Rem. Sens. Envir*. 180: 246-263. doi: 10.1016/j.rse.2016.02.038.

Picaut J., and T. Delcroix. 1995. Equatorial wave sequence associated with warm pool displacements during the 1986-1989 El Niño-La Niña. *J. Geophys. Res.* 100 (C9): 18393-18408. doi: 10.1029/95JC01358.

Picaut, J., E. Hackert, A. J. Busalacchi, R. Murtugudde, and G. S. E. Lagerloef. 2002. Mechanisms of the 1997 – 1998 El Niño – La Niña, as inferred from space-based observations. *J. Geophys. Res.* 107 (C5): 3037. doi: 10.1029/2001JC000850.

Qu, T., Y. T. Song, and C. Maes. 2014. Sea surface salinity and barrier layer variability in the equatorial Pacific as seen from Aquarius and Argo. *J. Geophys. Res*. 119: 15-29. doi: 10.1002/2013JC009375.

Qu, T., and J. Y. Yu. 2014. ENSO indices from sea surface salinity observed by Aquarius and Argo. *J. Oceanogr*. 70 (4): 367-375. doi: 10.107/s10872-014-0238-4.
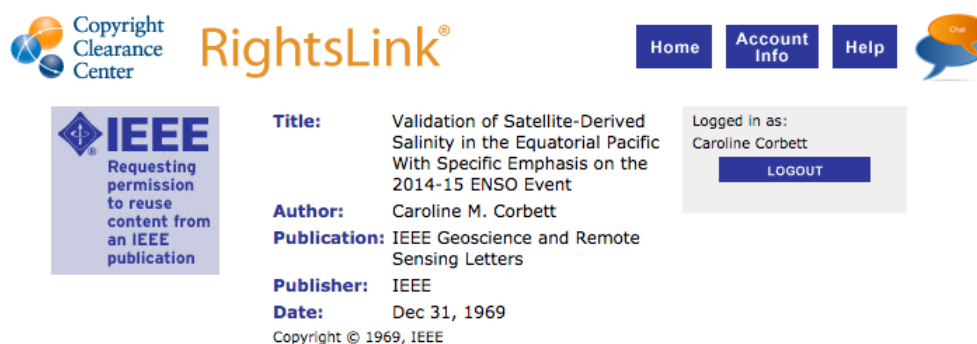
Rao, R. R., and R. Sivakumar. 2003. Seasonal variability of sea surface salinity and salt budget of the mixed layer of the north Indian Ocean. *J. Geophys. Res.* 108 (C1): 3009. doi: 10.1029/2001JC000907.

Ren, H. L., and F. F. Jin. 2011. Niño indices for two types of ENSO. *Geophys. Res. Lett.* 38: L04704. doi: 10.1029/2010GL046031.

Riser, S., L. Ren, and A. Wong. 2008. Salinity in Argo: A modern view of a changing ocean. *Oceanography* 21 (1): 56-67. doi: 10.5670/oceanog.2008.67.

Singh, A., T. Delcroix, and S. Cravatte. 2011. Contrasting the flavors of El Niño-Southern Oscillation using sea surface salinity observations. *J. Geophys. Res*. 116: C06016. doi: 10.1029/2010JC006862.

Song, Y. T., T. Lee, J. H. Moon, T. Que, and S. Yueh. 2015. Modeling skin-layer salinity with an extended surface-salinity layer. *J. Geophys. Res. Oceans* 120:1079-1095. doi: 10.1002/2014JC010346.

Spall, M. A. 1992 Variability of sea surface salinity in stochastically forced systems. *Clim. Dyn*. 8: 151-160. doi: 10.1007/BF00208094.

Taft, B. A., and W. S. Kessler. 1991. Variations of zonal currents in the central tropical Pacific during 1970 to 1987: sea level and dynamic height measurements. *J. Geophys. Res*. 96 (C7): 12599-12618. doi: 10.1029/91JC00781.

Trenberth, K. E .1997. The definition of El Niño. *Bull. Am. Meteorol. Soc*. 78: 2771-2777. doi: 10.1175/1520-0477(1997)078<2771:TDOENO>2.0.CO;2.

Trenberth, K. E., and D. P. Stepaniak. 2001. Indices of El Niño Evolution. *J. Clim.* 14: 1697-1701. doi: 10.1175/1520-0442(2001)014<1697:LIOENO>2.0.CO;2.

Vialard, J., P. Delecluse, and C. Menkes. 2002. A modeling study of salinity variability and its effects in the tropical Pacific Ocean during 1993-1999 period. *J. Geophys. Res.* 107 (C12): 8005. doi: 10.1029/2000JC000758.

Yu, L. 2011. A global relationship between the ocean water cycle and near surface salinity. *J. Geophys. Res.* 116: C10025. doi: 10.1029/2010JC006937.

APPENDIX A

COPYRIGHT PERMISSIONS

A.1. CHAPTER 2 COPYRIGHT PERMISSIONS

Copyright Clearance Center — RightsLink®

Home | Account Info | Help

Title: Validation of Satellite-Derived Salinity in the Equatorial Pacific With Specific Emphasis on the 2014-15 ENSO Event

Author: Caroline M. Corbett

Publication: IEEE Geoscience and Remote Sensing Letters

Publisher: IEEE

Date: Dec 31, 1969

Copyright © 1969, IEEE

Logged in as:
Caroline Corbett

LOGOUT

Thesis / Dissertation Reuse

The IEEE does not require individuals working on a thesis to obtain a formal reuse license, however, you may print out this statement to be used as a permission grant:

Requirements to be followed when using any portion (e.g., figure, graph, table, or textual material) of an IEEE copyrighted paper in a thesis:

1) In the case of textual material (e.g., using short quotes or referring to the work within these papers) users must give full credit to the original source (author, paper, publication) followed by the IEEE copyright line ⬥ 2011 IEEE.
2) In the case of illustrations or tabular material, we require that the copyright line ⬥ [Year of original publication] IEEE appear prominently with each reprinted figure and/or table.
3) If a substantial portion of the original paper is to be used, and if you are not the senior author, also obtain the senior author⬥s approval.

Requirements to be followed when using an entire IEEE copyrighted paper in a thesis:

1) The following IEEE copyright/ credit notice should be placed prominently in the references: ⬥ [year of original publication] IEEE. Reprinted, with permission, from [author names, paper title, IEEE publication title, and month/year of publication]
2) Only the accepted version of an IEEE copyrighted paper can be used when posting the paper or your thesis on-line.
3) In placing the thesis on the author's university website, please display the following message in a prominent place on the website: In reference to IEEE copyrighted material which is used with permission in this thesis, the IEEE does not endorse any of [university/educational entity's name goes here]'s products or services. Internal or personal use of this material is permitted. If interested in reprinting/republishing IEEE copyrighted material for advertising or promotional purposes or for creating new collective works for resale or redistribution, please go to http://www.ieee.org/publications_standards/publications/rights/rights_link.html to learn how to obtain a License from RightsLink.

If applicable, University Microfilms and/or ProQuest Library, or the Archives of Canada may supply single copies of the dissertation.

BACK | ⬥⬥⬥ | CLOSE WINDOW